Optical Imaging Modalities for Biomedical Applications

Atam P. Dhawan, Brian D'Alessandro, and Xiaolei Fu

Methodological Review

***Abstract*—Optical photographic imaging is a well known imaging method that has been successfully translated into biomedical applications such as microscopy and endoscopy. Although several advanced medical imaging modalities are used today to acquire anatomical, physiological, metabolic, and functional information from the human body, optical imaging modalities including optical coherence tomography, confocal microscopy, multiphoton microscopy, multispectral endoscopy, and diffuse reflectance imaging have recently emerged with significant potential for non-invasive, portable, and cost-effective imaging for biomedical applications spanning tissue, cellular, and molecular levels. This paper reviews methods for modeling the propagation of light photons in a biological medium, as well as optical imaging from organ to cellular levels using visible and near-infrared wavelengths for biomedical and clinical applications.**

***Index Terms*—Biomedical optical imaging, confocal microscopy, diffuse reflectance imaging, endoscopic imaging, fluorescence diffused optical tomography, microscopy, Monte Carlo simulation, multispectral imaging, optical coherence tomography, photoacoustic imaging, transillumination.**

I. Introduction

RECENT advances in biomedical imaging have made a revolutionary impact in diagnostic radiology and health care. In addition, the evolutionary growth in detector, instrumentation, and computing technologies have made medical imaging modalities capable of creating a comprehensive research and knowledge base for the better understanding of physiological processes. Computerized medical imaging and analysis methods using multiple modalities have facilitated early diagnosis, treatment evaluation, and therapeutic intervention in the clinical management of critical diseases.

Since X-ray radiographic imaging became a primary radiological diagnostic imaging method in the early part of the 20th century, there have been several advanced medical imaging modalities which have emerged and are available today to acquire anatomical, physiological, metabolic, and functional information from the human body. The most commonly used medical imaging modalities which are capable of producing multidimensional images for radiological applications include X-ray computed tomography (X-ray CT), magnetic resonance imaging (MRI) and its derivatives (such as functional and diffusion MRI), single photon emission computed tomography (SPECT), positron emission tomography (PET), and ultrasound. Each medical imaging modality uses a specific radiation (such as X-rays in X-ray CT) or energy (such as RF energy in MRI) depending on the underlying physics of imaging to obtain physiological information. In parallel, optical imaging methods including endoscopy and fluorescence imaging have been successfully used in clinical applications. Optical imaging is the oldest imaging method, well known for taking photographs of an object using the visible light spectrum of electromagnetic radiation. A simple form of optical imaging using fiber optics and a charge-coupled device (CCD) camera has been successfully used in endoscopy for imaging internal tissue structures with a narrow field of view. More recently, optical coherence tomography, confocal microscopy, and multispectral diffuse reflectance methods have been investigated for molecular and functional imaging, with innovative applications in biomedical research and targeted towards clinical applications.

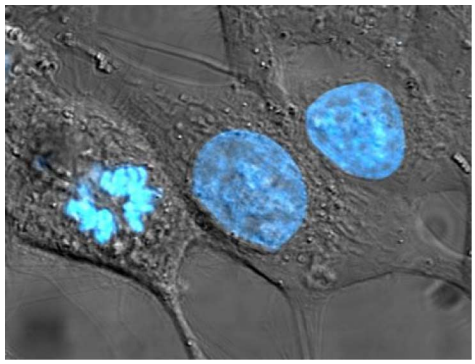

Fig. 1. Microscopic cellular image of stained HeLa cell nuclei [1].

It is interesting to note that although advanced medical imaging systems can be very expensive, optical imaging systems are relatively inexpensive, portable, noninvasive, and adaptable to acquire physiological and functional information from microscopic to macroscopic levels. Fig. 1 shows a microscopic optical image of stained HeLa cell nuclei for a pathological application. Table I summarizes clinical applications of the leading medical imaging modalities as well as optical imaging methods with their comparative resolution and

Manuscript received February 07, 2010; revised July 09, 2010; accepted September 14, 2010. Date of publication September 30, 2010; date of current version December 03, 2010. This work was supported in part by the George A. Ohl, Jr. Trust Foundation and the Gustavus and Louise Pfeiffer Research Foundation.

The authors are with the Department of Electrical and Computer Engineering, New Jersey Institute of Technology, Newark, NJ 07102 USA (e-mail: dhawan@adm.njit.edu; bmd5@njit.edu; xf5@njit.edu).

Digital Object Identifier 10.1109/RBME.2010.2081975

TABLE I
COMPARISON OF BIOMEDICAL IMAGING MODALITIES WITH RESPECT TO THEIR PENETRATION LEVEL, RESOLUTION AND COST. OPTICAL IMAGING MODALITIES ARE SHOWN WITH HIGHLIGHTED BACKGROUND

Medical Imaging Modality	Penetration Level	Resolution	Cost
X-ray Radiographs	Organ-Tissue	<mm	Low
X-Ray CT	Organ-Tissue	mm	Moderate
MRI	Organ-Tissue	mm	High
fMRI	Tissue-Cellular	mm	Very High
SPECT	Tissue-Cellular	mm	High
PET	Tissue-Cellular-Molecular	mm	Very High
Ultarsound	Organ-Tissue	<mm	Low
Optical Microscopy	Tissue-Cellular	micron	Low
Fluroscence Microscopy	Cellular-Molecular	micron	Low
Confocal Microscopy	Tissue-Celleular-Molecular	micron	Low-Moderate
Endoscopy	Tissue	micron	Low
Optical Coherence Tomogrpahy	Tissue-Cellular	micron	Moderate
Diffuse Reflectance	Cellular-Molecular	micron	Low

cost assessment. For example, optical coherence tomography (OCT) is a noninvasive imaging technique capable of producing high resolution cross-sectional images through inhomogeneous samples. It offers a resolution level much higher than current MRI, CT, SPECT, PET, and ultrasound technologies. Though primary optical imaging modalities such as endoscopy have been used in the clinical environment for several years, the clinical perspective of other advanced optical imaging modalities has yet to be established in diagnostic radiology. Recent advances in endoscopy, optical coherence tomography, confocal microscopy, fluorescence imaging and multispectral transillumination technologies clearly show great potential in becoming the mainstream diagnostic and treatment evaluation technologies of the future.

In this paper, we first present an overview of modeling the propagation of visible light and near-infrared (NIR) photons in a biological turbid medium for imaging. A chronology and review of optical imaging technologies is then presented with continuously growing interests in biomedical applications.

II. LIGHT PROPAGATION IN BIOLOGICAL TURBID MEDIUM

Optical imaging modalities may utilize the visible light spectrum from 400 to 700 nm of electromagnetic radiation to produce visible images in biomedical applications such as microscopy, endoscopy, and colonoscopy. However, the excitation and emission spectrum in advanced optical imaging modalities is not restricted to the visible spectrum, but can be extended out on both sides into the soft ultraviolet (< 400 nm) and near-infrared [(NIR) > 700 nm] range for fluorescence and multispectral imaging applications. The visible light spectrum, along with soft ultraviolet and NIR bands, follows relatively stochastic behavior in photon interaction and propagation in a heterogeneous multilayered biological tissue medium. Unlike X-ray photons, optical photons do not penetrate the entire biological tissue medium with predominantly straight transmission. Electromagnetic theories of light reflection, refraction, diffusion, interference, and propagation are described in depth

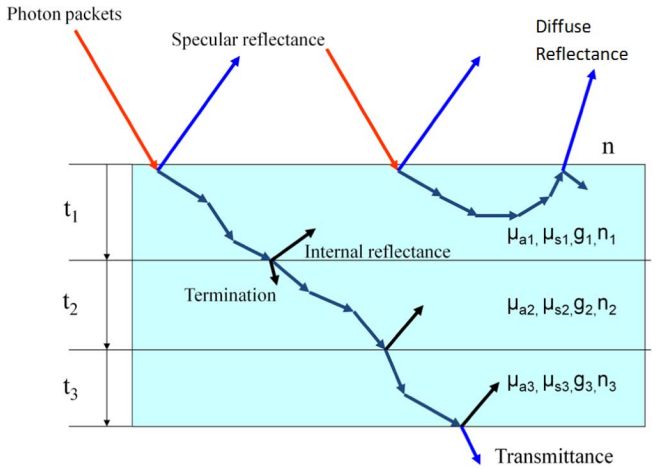

Fig. 2. Simplified model of biological medium with three layers. Each layer is associated with absorption coefficient μ_a, a scattering coefficient μ_s, an anisotropic factor g, and a refractive index n.

by Born and Wolf [2] and are also discussed in recent books [3]–[5].

Light radiance is characterized by the total emission or reflection within a solid angle. It is the sum of all spectral radiances at individual wavelengths. As light passes through a heterogeneous multilayered medium, it suffers from wavelength dependent absorption and scattering events. In a multilayered heterogeneous medium such as a biological tissue, characteristic absorption and scattering coefficients determine the light radiance at a given point. It is also described by the scattering phase function, which is defined as the cosine of the angle between the incident and scattered paths. The weighted average of the scattering phase function is called the anisotropy factor. In a biological tissue, the anisotropy factor is strongly peaked in the forward direction. However, a series of scattering events in a turbid medium with a continuously changing direction of light propagation can also produce backscattered diffused radiance which can reemerge from the surface [6]–[8]. Fig. 2 shows a simple model of a multilayered biological tissue medium. For

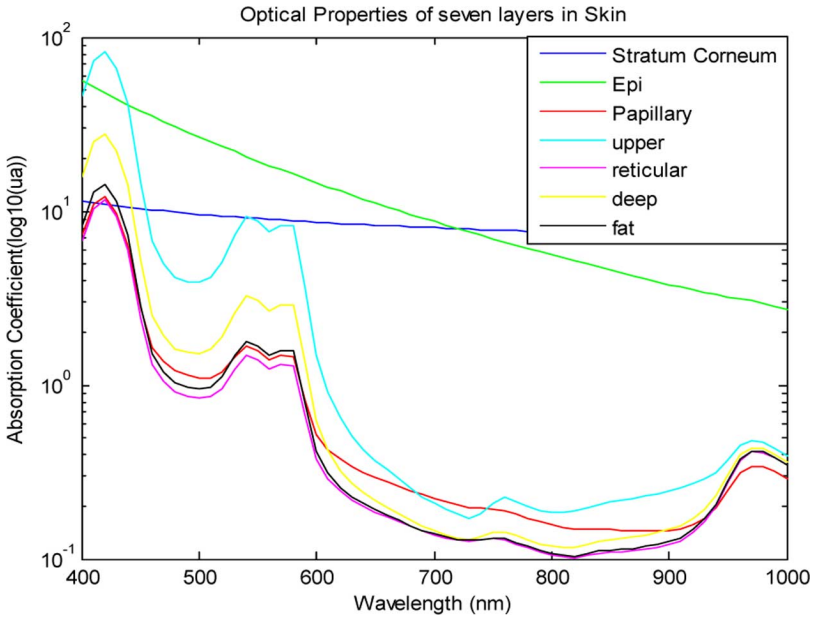

Fig. 3. Wavelength dependent absorption spectra of seven-layer model of skin and subcutaneous fat.

simplicity, each layer is assigned average absorption and scattering coefficients, an anisotropy factor, and an index of refraction. It should be noted that these optical parameters for biological tissues are wavelength dependent and have been investigated by many researchers. For example, a seven-layer model of skin with absorption and reflectance spectra in the visible and near-infrared spectral regions is presented and analyzed by Meglinski *et al.* [9]. Fig. 3 shows the wavelength dependent absorption spectra for a seven-layer tissue model of skin and subcutaneous fat. Light transmission in a turbid heterogeneous biological medium, also called a random biological medium, is governed by radiative transport theory [10], [11] for which the Green's function is widely used to find a solution.

Optical imaging through surface reflectance follows basic principles of reflection, refraction, and scalar wave theory. From the incident light, some photons are reflected by the air-tissue surface interface [for example, the stratum corneum of the skin, if a skin lesion is being imaged through epi-illumination light microscopy (ELM)] [12]. Remaining photons enter the multilayered turbid tissue medium following the basic laws of radiative transfer that can be represented by Maxwell's equations. The radiative transfer theory in a random medium is also called the transport theory of light propagation. Optical radiation diffuses in a large random medium by propagating as planar and even spherical waves. Analytical solutions to the radiative transfer theory have been attempted but are quite difficult to compute due to the complex nature of the transport equation. As a result, approximations to the transport equation have been used which are easier to solve, such as the Fokker–Planck equation as well as a modification of that equation proposed by Leakeas and Larson [13], [14]. Many investigators have used the Green's function on the radiative transport and Fokker–Planck equations to compute the point spread function in a half-space composed of a uniform scattering and absorbing medium [2]. Diffusion theory has also been used as an approximation of the radiative transport equations to describe light propagation in a turbid medium [11], [15]. This alternative has been widely popular because of its simplicity, specifically to model time-resolved light propagation with physical constraints. However, diffusion theory assumes a constant scattering phase function, which is not necessarily accurate for a biological medium since it is typically anisotropic with a sharply forward peaked phase function but a directionally dependent point spread function. In addition to multiple reflections and refractions in a multilayered biological medium, optical photons suffer from wavelength/energy dependent absorption through elastic and inelastic scattering events that are isotropic as well as anisotropic in nature.

Photon transport and propagation in an absorbing medium can be modeled analytically by the radiative transfer equation through total radiance L defined as the spectral radiance $L_v(\vec{r}, \widehat{s}, t)$ integrated over a narrow band of frequencies $[\nu, \nu + \Delta\nu]$ as [2]–[4], [16]

$$L(\vec{r}, \widehat{s}, t) = L_\nu(\vec{r}, \widehat{s}, t)\Delta\nu \tag{1}$$

where $\vec{r}$ is the position vector, $\widehat{s}$ is the unit direction vector, and t represents time.

The spectral radiance $L_v(\vec{r}, \widehat{s}, t)$ is defined as the light energy flow per unit normal area (perpendicular to the flow direction) per unit solid angle per unit time per unit frequency bandwidth.

The fluence rate $\Phi(\vec{r}, t)$, defined as the energy flow per unit area per unit time, can be expressed over the entire solid angle Ω as

$$\Phi(\vec{r}, t) = \int_{4\pi} L(\vec{r}, \widehat{s}, t) d\Omega. \tag{2}$$

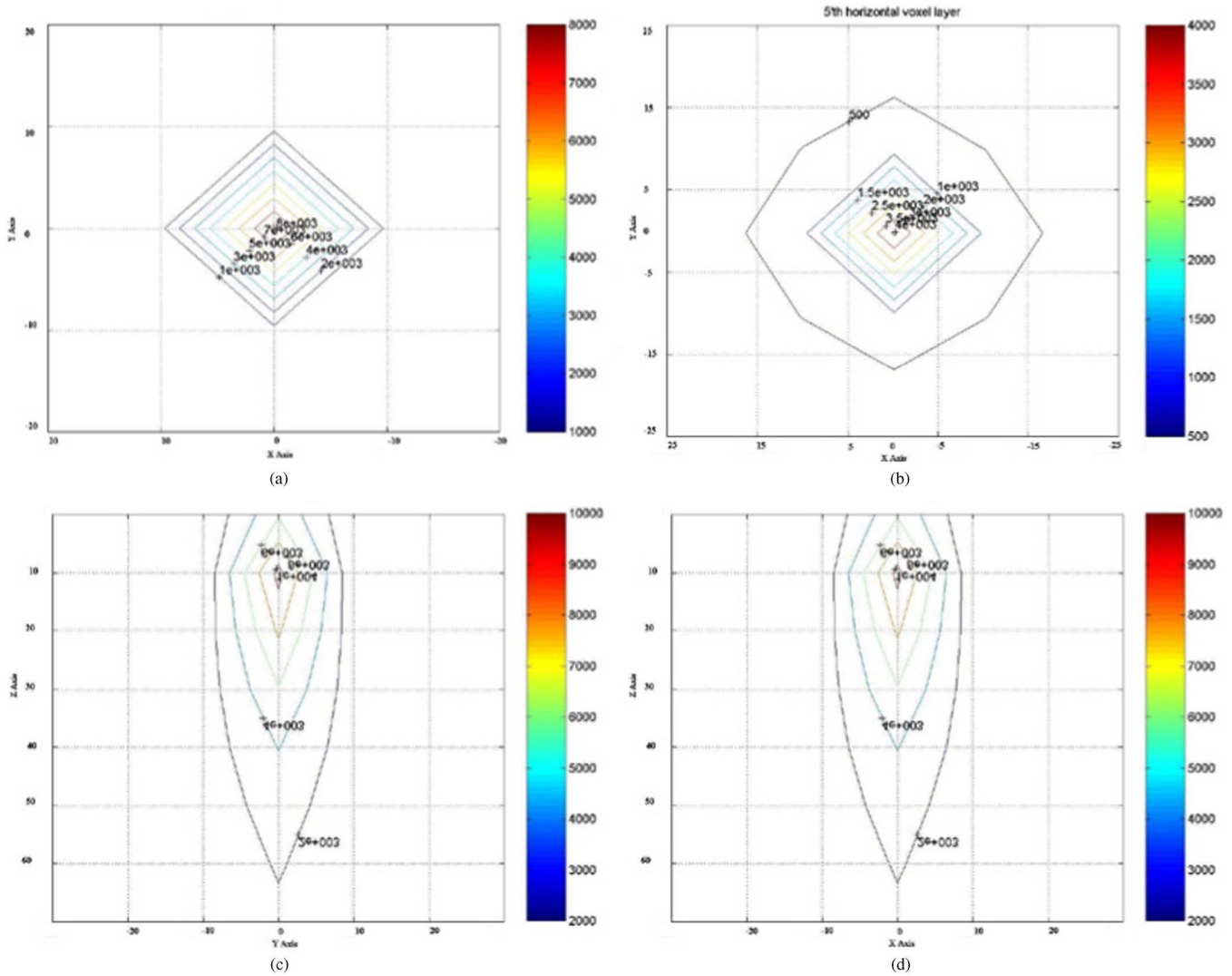

Fig. 4. Photon energy distribution curves in biological medium that is illuminated through two point sources incident perpendicular to the tissue model with 10-μm cubical voxels: (a) and (b) for the second and seventh voxel layer parallel to the tissue surface, (c) for the Y-Z plane passing through the point of incidence, and (d) for the X-Z plane passing through the point of incidence. Axis dimensions in all plots are in terms of voxel indices [36]. (a) XY plane at $Z = 10$–$20\ \mu$m. (b) XY plane at $Z = 70$–$80\ \mu$m. (c) YZ plane at $X = 0$. (d) XZ plane at $Y = 0$.

From the above, it can be shown that the specific absorption in the light energy can be obtained as [2]–[4], [16]

$$A(\vec{r}) = \int_{-\infty}^{\infty} A_p(\vec{r}, t)dt \tag{3}$$

where the specific absorption rate $A_p(\vec{r}, t)$ is given as

$$A_p(\vec{r}, t) = \mu_a \Phi(\vec{r}, t) \tag{4}$$

where μ_a is the absorption coefficient of the medium.

It is usually difficult to analytically solve the radiative transport equation due to a number of independent variables. The basic radiative transport equation is thus simplified using the diffusion approximation that the biological medium is not only an absorbing medium, but it also contains heterogeneous molecules which cause significant scattering. It is assumed that the absorption coefficient in a biological scattering medium is much smaller than the scattering coefficient, and the medium is nearly isotropic after scattering events. Using an expansion of radiance in (1) and limiting the coefficients to first-order spherical harmonics allowing only a fractional change in one transport mean free path, it can be shown that fluence rate can be expressed with much less complexity through the diffusion equation as [3], [16]

$$\frac{\partial \Phi(\vec{r}, t)}{c\partial(t)} + \mu_a \Phi(\vec{r}, t) - \nabla \cdot [D \nabla \Phi(\vec{r}, t)] = S(\vec{r}, t) \tag{5}$$

where S is an isotropic source distribution and D is a diffusion constant that can be described using the Fick's law for diffusion of light photons in a scattering medium [16] as

$$D = \frac{1}{3(\mu_a + \mu_s(1 - g))} \tag{6}$$

where μ_a and μ_s are absorption and scattering coefficients and g is the anisotropic factor of the medium.

Maxwell's equations, the transport equation, and the diffusion equation have been applied for biological imaging applications at the microscopic, mesoscopic, and macroscopic scales, respectively. For small volumes, analytical or numerical solutions of the Maxwell's equations have been used to model the light propagation in a random medium. For large volumes the diffusion equation can be solved, but for intermediate volumes the transport theory has been applied using the Monte Carlo simulation method [17]–[20].

As mentioned previously, visible and NIR optical wavelengths suffer from multiple reflections and scattering in addition to absorption when propagated into random biological media. This causes uncertainty in the photon distribution paths between the source and detector. Hence, the problem of reconstructing the perturbation profile from scattered radiation is not simple. Usually, numerical and analytical solutions are based on gross approximations that are inconsistent with physical conditions and constraints. Therefore, to reconstruct images of a biological turbid medium, a forward model based on the imaging geometry and pre-assumed approximations of the biological medium with distributions of optical photons in the modeled medium is used to find the inverse solution (the reconstructed images of the known medium). Since feasible solutions are obtained by the basic theory of radiative transfer, propagation of light can be modeled using the Monte Carlo simulation method [17], [18], [20].

A. Monte Carlo Simulation of Light Propagation in Biological Medium

Monte Carlo simulation is a statistical technique for simulating random processes and has been applied to light-tissue interactions under a wide variety of situations [15], [17]–[24]. Photon interaction with matter via scattering and absorption is stochastic in nature and can be described using Monte Carlo methods by appropriately weighting absorption and scattering events [15]. Laser irradiation of skin using homogeneous [25] and layered geometries [21], [22] has been simulated using Monte Carlo methods. In addition, for light propagation in highly scattering tissue-like media, the results of the diffusion approximation to the radiative transport equation have been compared to Monte Carlo simulation results [17]. The Monte Carlo approach is in close agreement with the results of independent radiative transfer calculations [26], while the diffusion models examined [27], [28] were inaccurate for predicting some of the characteristics of light fluence distributions.

The most commonly simulated tissue models used in Monte Carlo simulations assume tissues to be layered structures with homogeneous properties within each layer [18]–[21]. Although these models are simple and easy to implement, real tissues are more complex geometrically and consist of nonhomogeneous layers. Thus, a modular representation of the tissue architecture is a more appropriate method for capturing variations in the tissue structure. Two primary methods, shape-based and voxel-based, have been used to represent an object in a mathematical simulation. The shape-based approach [29] describes the boundaries of each object using mathematical equations. However, in these shape-based methods, irregular boundaries are difficult to describe mathematically. The voxel-based approach [24] represents an object as a set of voxels. The accuracy with which irregular boundaries can be described using the voxel-based approach depends on the size of the voxels.

Monte Carlo methods simulate the light propagation in a turbid multilayered medium with a photon step size S which is dependent on the absorption and scattering coefficients within the tissue voxel and is calculated randomly from a logarithmic distribution of path lengths. The step size is calculated as

$$S = \frac{-\ln(\xi)}{(\mu_a + \mu_s)} \tag{7}$$

where μ_a is the local absorption coefficient, μ_s is the scattering coefficient, and ξ is a random number uniformly distributed in the interval $[0, 1]$.

The photon interacts with the tissue after propagating the path length equal to the step size. The tissue absorbs some part of the photon weight during the interaction, which is given by

$$\Delta W = \frac{\mu_a}{\mu_a + \mu_s} W \tag{8}$$

where the sum of μ_a and μ_t is the tissue interaction or transport coefficient in the tissue voxel.

The new direction of the photon after interacting with the tissue is calculated by a random selection of the azimuthal and deflection angles. The azimuthal angle φ is independent of the tissue properties and is uniformly distributed over the interval $[0, 2\pi]$. The value of the azimuthal angle is based on selection of another random number ξ and is calculated as

$$\varphi = 2\pi\xi. \tag{9}$$

The deflection angle $\theta (0 \leq \theta \leq \pi)$ is sampled statistically using the probability distribution of the cosine of the deflection angle, $\cos\theta$, described by the scattering function. Using the scattering function proposed by Henyey and Greenstein [30], the probability distribution of $\cos\theta$ is

$$p(\cos\theta) = \frac{1 - g^2}{2(1 + g^2 - 2g\cos\theta)^{3/2}} \tag{10}$$

where the anisotropy factor g, which is dependent on the scattering characteristics of the tissue, is equal to $\langle\cos\theta\rangle$ and has a value between -1 and 1. For isotropic scattering, the anisotropy factor is equal to 0; for forward directed scattering the anisotropy factor is equal to 1. The cosine of the deflection angle can be calculated by selecting another random number ξ given the following equations:

$$\begin{aligned} \cos\theta &= \frac{1}{2g}\left[1_\xi + g^2 - \left(\frac{1 - g^2}{1 - g + 2g}\right)\right] \quad \text{if } g \neq 0 \\ \cos\theta &= 2\xi - 1 \quad \text{if } g = 0 \end{aligned} \tag{11}$$

where ξ is a random number uniformly distributed in the interval [0,1].

During its propagation, if the photon comes across a boundary where the refractive index changes, a decision about internal reflectance or transmittance is made based on the internal reflectance parameter $R(\alpha_i)$ calculated using Fresnel's formula [2], [31] as

$$R(\alpha_i) = \frac{1}{2}\left[\frac{\sin^2(\alpha_i - \alpha_t)}{\sin^2(\alpha_i + \alpha_t)} + \frac{\tan^2(\alpha_i - \alpha_t)}{\tan^2(\alpha_i + \alpha_t)}\right] \qquad (12)$$

where α_i is the angle of incidence of the photon with the boundary and α_t is the angle of transmission. By generating a random number ξ uniformly distributed in the interval [0,1] and comparing it with the internal reflectance parameter $R(\alpha_i)$, we determine whether the photon is internally reflected. If $\xi \leq R(\alpha_i)$, the photon is internally reflected; otherwise, the photon is transmitted through the boundary.

When the photon weight becomes less than a threshold value due to absorption by the tissue, further propagation of the photon yields little information. To terminate photons whose weight is below the threshold value and also to ensure conservation of energy, a Russian Roulette technique is used to determine if the photon should be terminated [32], [33]. This technique gives a photon one chance in m of surviving with a weight of mW_r, where W_r is the present weight of the photon. A random number ξ uniformly distributed in the interval [0,1] is compared with $1/m$ and the photon survives if $\xi > 1/m$. This method conserves energy yet terminates photons in an unbiased manner. A photon is also terminated when it escapes the tissue by transmission across a tissue boundary. If the photon escapes through the upper boundary on which the light is initially incident and is collected by the detector array above the tissue, then the photon weight is added to the diffuse reflectance. Likewise, if the photon escapes through the lower boundary and is collected by the detector array on the bottom of the tissue, then the photon weight is added to the transmission.

In a voxel-based simulation, the photon is transported voxel-by-voxel within the medium. Therefore, checking the boundary conditions at every voxel interface as explained above is computationally expensive. To improve simulation efficiency, Sato and Ogawa [34] suggested a photon accelerating method to check for layer or object boundaries by comparing the refractive indices of all the voxels within the photon path for a distance equal to the step size. If all of these voxels have the same refractive index, then the photon is free to move the entire step size and interact with the tissue. On the other hand, if the refractive index changes along the photon path, then an object boundary is present and its distance from the existing photon location is calculated and compared with the step size. If the step size is smaller than the boundary distance, the photon can take this step; otherwise, the photon is moved to the boundary where it can be reflected or transmitted. The photon accelerating method improves the simulation efficiency as only two checkpoints are used before the photon-tissue interaction proceeds, regardless of the number of voxels crossed by the photon. Computational efficiency can be further improved by using the three-dimensional material grid array that is stored as a series of two dimensional arrays parallel to the surface of the medium [35].

Fig. 4 shows a visualization of a Monte Carlo simulated photon path between detectors and sources for a diffuse reflectance based imaging geometry in which the detectors are placed between two sources [36]. Monte Carlo simulation is a powerful tool for estimating otherwise difficult solutions. Using the techniques of Monte Carlo simulation, the propagation of light through biological media can be modeled. This provides a basis for the simulated study of optical imaging modalities in order to better understand the images obtained. The various optical imaging modalities and their methods and applications will be discussed in Section III.

III. Optical Imaging Modalities

Although a wide variety of optical imaging modalities are available, it is important to note that for specific cellular and tissue imaging, as well as for spectroscopy applications, a combination of these optical imaging methods is being investigated for joint use in clinical diagnostic evaluations. For example, endoscopic imaging and spectroscopy have been successfully used together in clinical and surgical applications, specifically for respiratory (associated with esophagus and lungs), gastrointestinal, tissue perfusion, and blood flow imaging applications [37].

Mainstream optical imaging modalities can be categorized into the following groups:

1) microscopic imaging modalities: microscopy, confocal microscopy, fluorescence microscopy, and multiphoton microscopy;
2) endoscopic imaging modalities: optical endoscopy and spectroscopy;
3) optical coherence tomography;
4) diffuse reflectance and transillumination imaging.

A. Microscopic Imaging Modalities: Microscopy, Confocal Microscopy, Fluorescence Microscopy, and Multiphoton Microscopy

Microscopic imaging modalities provide a variable magnification and depth of field for imaging a tissue in an embedded medium or *in vivo*. The magnification power provides the capability to image the tissue at the cellular level. The distance to which an optical system can clearly focus is known as the depth of field. Within the depth of field, objects are in focus; that is, they appear crisp and sharp. At increasing distances outside the depth of field (either closer to or further away from the camera), objects gradually become more blurred. In typical photography, an image is comprised of the superposition of all the light originating from all depth planes, thus providing a wide field of view typical to what a human's eyes can see. For biological imaging, however, it is often desired to obtain separate images of individual depth planes. This is known as optical sectioning. In confocal microscopy, a small pinhole is used to block all out of focus light, therefore limiting the image only to the light which is reflected from objects in the focal plane. Multiphoton microscopy, on the other hand, is designed in such a way that light is only emitted back from the current point of interest.

These techniques are often used to image the fluorescent light emitted from biological tissue on a slice by slice basis.

Fluorescence imaging uses ultraviolet light to excite fluorophores and then collect back emitted light at a higher wavelength. Fluorophores include endogenous and exogenous fluorophores. The former refers to natural fluorophores intrinsic inside tissue such as amino acids and structural protein, and these fluorophores are typically randomly distributed. The latter usually refers to smart polymer nanoparticles targeting specific molecules such as hemoglobin.

Due to the disparity of the metabolism states, certain kinds of exogenous fluorophores have unique distributions in malignant tissue compared to those in normal tissue. Thus, detection of these distributions may be used to suggest the presence of a cancer. Fluorescence imaging has a similar mechanism as single particle emission computed tomography (SPECT). Aspiring results have been obtained by several groups [38], [39].

B. Confocal Microscopy

As mentioned previously, confocal microscopy (CM) achieves optical sectioning through the use of a pinhole. This pinhole is located at the focus point just before the detector, which blocks all but the in-focus light from the imaging plane from reaching the detector (see Fig. 5). Imaged light is thus limited only to that which is reflected from objects in the focal plane, a rather slim optical section of 3-D space. For opaque or transparent objects such as biological tissue, this allows imaging of only one slice of the object at a time, an incredibly useful tool for imaging the interiors of volumes otherwise difficult to see by conventional microscopy. Employing a laser to scan over an object one pixel and slice at a time is known as confocal laser scanning microscopy (CLSM), and this method can be used to digitally image a comprehensive 3-D image volume. Confocal microscopy thus can obtain high resolution, slice-by-slice images of tissue *ex vivo* or *in vivo*. This technique is used in a wide variety of applications, including the imaging of normal tissue for morphological and structural investigation, and the imaging of lesions with an aim towards improved diagnosis.

Confocal microscopy is typically seen as a faster and more convenient alternative to physically slicing a biopsy for conventional microscopic evaluation. A histological examination of skin lesions, for example, is the gold standard for melanoma diagnosis, but its pitfalls include unnecessary biopsies, sampling error, and risk of scarring. The procedure is also time consuming and it eliminates the possibility of observing dynamic changes over time. Histological analysis of a biopsied region also sometimes involves tissue processing and staining which can hinder tissue analysis. Tissue distortion may occur due to manipulation and processing artifacts, such as tissue dehydration and shrinkage of the biopsy [41]. Preparing glass slides for conventional microscopic examination takes multiple days, whereas laser scanning confocal microscopy can be applied to fresh specimens for immediate examination after a biopsy [42]. Thus, there are good reasons to pursue a method of slice by slice imaging which is noninvasive and avoids the problems associated with conventional techniques, but still maintains the detail needed for proper pathological analysis. The two main areas of research using various types of confocal microscopy are: 1) the use of sectioned images to investigate structural and morphological properties of tissue and 2) the use of these structural features to differentiate between normal and abnormal cells for a more accurate diagnosis.

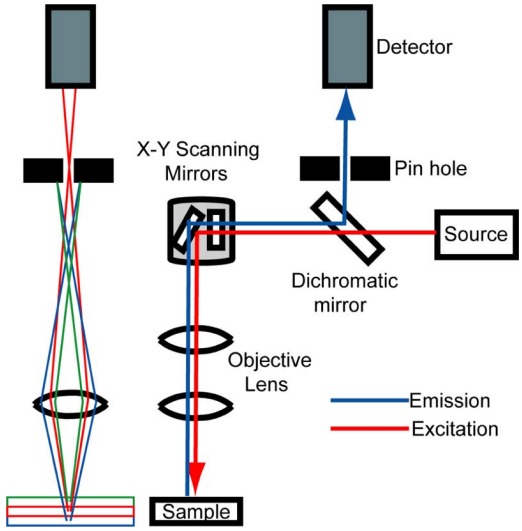

Fig. 5. Left: schematic of confocal microscope principle. Pinhole aperture placed at focal length of lens blocks light coming from out-of-focus planes (green and blue lines), while allowing light coming from in focus plane to reach detector. Right: Schematic of point-scanning fluorescence confocal microscope. Dichromatic mirror reflects the emission light while allowing excitation light to pass through. Motorized X–Y scanning mirror pair is used to collect data from selected sample area (with permission from Patwardhan *et al.* [40]).

C. Tissue Imaging With Confocal Microscopy

Initial studies generally seek to analyze what level of detail can be obtained through confocal microscopy, and it has been determined that even for a wide variety of imaging sites (such as corneal nerves [43], the skin [44], and fluorescent imaging of the GI tract [45]), the structure, distribution, and morphology of confocal microscopic images compare excellently to histology. Thus, confocal microscopy is a feasible method for cellular and subcellular imaging.

Confocal microscopy is especially suitable for investigative studies on the skin, since the depth range of CM is around 200–300 μm, which is enough to encompass the many different layers of skin. This method is painless, does not harm the tissue, and is feasible for repeated imaging of the skin on a slice by slice basis. These images allow the visualization of cellular and nuclear structure, the identification of different skin layers, as well as the visualization of sebaceous glands, hair follicles, and sweat ducts, all of which correlate very well with histology. Morphometric variations in normal skin between sun-exposed and sun-protected sites have even been observed, for a variety of different characteristics [46]. Confocal microscopy can image corneocytes, keratinocytes, epidermal walls, spinous cells, basal keratinocytes, circulating blood cells, and extracellular matrix fibers [41]. It has been found that using CLSM, image contrast arises due to differences in the backscattered light from structures in the skin. Structures such as melanin and the cytoplasm have different refractive indices and consequently

reflect back different amounts of light to the detector. Thus, homogeneous layers such as the stratum corneum show little contrast and are darker, while heterogeneous layers such as the viable epidermis show high contrast and are brighter. This results in a well-defined visible junction between the stratum corneum and the viable epidermis [47].

Investigations using CM have a far broader scope than just the skin, however. The technique has been used to study fluorescent drug transport in isolated brain capillaries [48], as well as to analyze pancreatic islet architecture and composition [49]. Confocal microscopy has also been used to estimate the scattering coefficient in different layers of cervical epithelium. Different layers exhibit different scattering coefficients, and scattering varies when dealing with dysplastic tissue as well. Thus, optical tissue models which assume that scattering is homogenous throughout the medium are not necessarily accurate [50]. There is clearly a wealth of information that can be obtained through optical biopsy, as it allows slice by slice visualization along the depth of tissue.

New technological techniques as well as perhaps the combination of confocal microscopy with other tools may be able to help bring CM to more standard usage. For example, use of a MEMS scanner for dual axis confocal microscopy was demonstrated with a small design especially suited for endoscopic applications [51]. Confocal microscopy has also been combined with Raman Spectroscopy to obtain information about the molecular composition of the skin at different depths. Since CM enables the isolation of light emitting from a particular slice below the surface, only this slice is spectrographically analyzed. This combination technique provides a way to study the water concentration profile as a function of depth within the tissue. It can also be used to analyze, *in situ*, the molecular composition of specific skin structures such as the sweat duct, and consequently the composition of sweat within a sweat duct. The method may also have a potential application in blood analysis to find the local hemoglobin-oxygen saturation [47].

D. Confocal Microscopy for Diagnostic Applications

In studies related to diagnostic application of confocal microscopy, current research has shown that it is possible to differentiate between normal and abnormal cells in confocal images of a biopsy specimen [52]. The accuracy for detecting cancer in esophagus, stomach, and colon specimens has been reported as 89.7% using confocal microscopy [42]. A "virtual histology" on colorectal lesions has found differences in visualization of cell nuclei depending on the grade of dysplasia [53].

While the method is useful for immediate biopsy imaging, the true advantage of confocal microscopy is its ability to noninvasively image tissue *in vivo*, especially for the skin, eye, and gastrointestinal tract. This can be helpful for guided surgical procedures, such as a biopsy, and it also increases efficiency due to the instant observation of possible pathologies. For example, due to the difficulties in differentiating benign and premalignant lesions of the oral cavity, a laser confocal endomicroscope was used to perform *in vivo* fluorescence imaging. Structural differences could be distinguished between normal and lesion tissue, thus showing potential as an imaging method for the oral cavity [54].

Confocal microscopy can also be used to realize morphological differences in proliferative skin lesions, non-melanoma skin cancer, malignant pigmented skin lesions, and dysplastic nevi [41]. A recent study was performed using CM images of 102 melanocytic lesions, with an average of 163 images per lesion at three different depth levels. Based on a feature analysis of these images, six criteria were developed and used to score each lesion towards a melanoma diagnosis. This method resulted in an overall sensitivity of 97.3% and specificity of 72.3%. Examination was time consuming because the field of view is small and three depth levels are used, but for difficult or inconclusive cases this method may be helpful [55].

E. Fluorescence and Multiphoton Fluorescence Microscopy

While confocal microscopy is a useful tool for optically sectioned imaging, the use of a pinhole to block out of focus light creates an inherent drawback in that much of the emitted fluorescent information is lost. Since only a fraction of the fluorescent light is able to pass through the pinhole, the source intensity must be high enough so that there is enough fluorescent signal available to be detected. This can create other problems such as photobleaching and photodamage, and imaging depth is limited. To overcome these challenges, multiphoton fluorescence microscopy has been developed as an incredibly useful nonlinear optical imaging technique, which has shown significant promise in tissue characterization and molecular imaging.

The diffusion equation presented above as (5) can be described per excitation wavelength (representing subscript x) of the illumination source used for fluorescence imaging and tomography as

$$\frac{\partial \Phi_x(\vec{r},t)}{c\partial(t)} + \mu_{ax}\Phi_x(\vec{r},t) - \nabla\cdot[D_x\nabla\Phi_x(\vec{r},t)] = S_x(\vec{r},t). \quad (13)$$

The fluorescence emission can also be described by a similar diffusion equation for fluorescence emission wavelength with a subscript m as

$$\frac{\partial \Phi_m(\vec{r},t)}{c\partial(t)} + \mu_{am}\Phi_m(\vec{r},t) - \nabla\cdot[D_m\nabla\Phi_m(\vec{r},t)] = S_m(\vec{r},t). \quad (14)$$

The source term can now be obtained using the following convolution [3], [38], [56], [57]:

$$S_m(\vec{r},t) = \int_0^t y(t-t')\mu_{afx}\left[\Phi_{px}(\vec{r},t') + \Phi_x(\vec{r},t')\right]d't \quad (15)$$

where y is the yield of fluorescence emission and μ_{afx} is the absorption coefficient of the target fluorophores at the excitation wavelength.

The above theoretical formulation may be used in quantitative analysis and interpretation of fluorescence emission based microscopic images.

F. Multiphoton Fluorescence Microscopy

First described by Denk, Strickler, and Webb in 1990 [58], multiphoton microscopy has quickly become a standard tool

in biological optical imaging. Similar in objective to confocal microscopy, multiphoton microscopy can isolate optical sections in order to image tissue one depth slice at a time. Rather than using a pinhole to block all out of focus light beams, multiphoton microscopy relies on the fact that multiple photons of longer wavelengths can simultaneously interact with a fluorophore to create the same excitation that a single photon of a shorter wavelength would create. As long as the total energy required to excite the fluorophore is met, it does not matter if the energy comes from a single photon of high energy or multiple photons each of lower energy. Typically in practice, two photons are used (each providing half of the required excitation energy) and this technique is known as two-photon microscopy. However, to ensure that lower energy photons interact simultaneously with the same fluorophore, it is essential that the photon density be very high. Fortunately, this requirement is just the case at the focal point of a microscopy system. Only at that point, where photons are concentrated into a small volume, do multiple photons have the density required to properly interact with and simultaneously excite the fluorophore. In this way, one point at a time is imaged in a 3-D volume, thus providing the needed optical sectioning. Since the rate of excitation in two photon microscopy depends on the average squared photon density, the photon density everywhere other than the focal point is far too low to foster fluorescent excitation. This ensures that there can be no interfering light from out of focus planes. Multiphoton fluorescent microscopy has advantages over confocal microscopy in that since a pinhole is not required, no emitted fluorescent light is blocked from being detected. Also, there is reduced photobleaching and photodamage from light outside the focal plane and reduced scattering of incident light. Since the source photons are of a longer wavelength than confocal microscopy, they penetrate deeper into biological tissue, thus providing an increased depth of imaging [59]–[65].

G. Functional Multiphoton Microscopy

Because of its high resolution at the cellular and subcellular level, as well as the ease of obtaining 3-D reconstructions, multiphoton microscopy is also often used for functional imaging, that is, the spatial and temporal visualization of biological processes in living cells [66]. Two photon microscopy has been applied to obtain a 3-D visualization over time of the accumulation and penetration of nanoscale drug vehicles within the skin [67], the cellular dynamics of immunology [68], mouse kidney development [69], as well as neuronal dendrite dynamics [70].

Still, one of the drawbacks of using two-photon fluorescence is its limited temporal resolution, due to the time needed to move the mirrors directing the laser beam over a two dimensional area. In an investigation performed by Masters, *et al.*, confocal microscopy was compared with two-photon microscopy. It was found that two photon imaging had an enhanced overall contrast and allowed more structures to be visualized compared with CM, such as corneocytes in the stratum corneum and collagen and elastin fibers in the dermis. However, CM could be imaged at video rates, while two-photon microscopy was significantly slower than needed for real time video [71]. A high temporal resolution is important for observing functional dynamics as well as fast physiological events. Faster imaging can be achieved if the laser is constrained to only one dimension, that is, scanning back and forth in a straight line; but this of course limits the spatial resolution. To overcome this limitation, multiple single line scanning has been used to simultaneously image a series of 1-D lines, thus producing a 2-D image at a much higher speed [72]. Another solution has been to utilize an acoustic-optical deflector system, whose nonmechanical nature allows for faster scanning [73]. The acousto-optic deflectors can even be extended to ultra fast scanning in three dimensions, as has been demonstrated to obtain live functional imaging of neuronal dendrite dynamics [70].

H. Recent Advancements

While multiphoton microscopy is an extraordinarily useful tool for imaging tissue, it is often limited to easily accessible regions of the body. While it is possible to investigate other regions, this usually involves surgery to excise the tissue, or it requires cultured cells or isolated primary cells. Either way, imaging occurs outside of the living body, which may or may not represent true *in vivo* tissue, especially for functional imaging. *In vivo* imaging of cell behavior is always best, although often difficult. To overcome this challenge, two-photon microscopy has been used to image an externalized kidney still attached to a living animal, in order to study functional and physiological aspects of the kidney [74]. Likewise, a needle-like gradient index lens only 350 μm in diameter has been used to probe deep brain tissue (such as the cortical layer V and the hippocampus) of mice *in vivo* [75].

Further improvements are being developed for the use of multiphoton microscopy in a miniaturized endoscopic system [76]–[79]. Some challenges for *in vivo* endoscopic imaging using multiphoton microscopy include chromatic dispersion of the femtosecond pulses through the fiber, as well as reducing the probe head size. Endoscopes built with single mode fiber have difficulty utilizing multiphoton imaging technology because of group-velocity dispersion and self-phase modulation. Jung *et al.* was able to overcome this by using microendoscope probes based on gradient-index lenses [65]. Different types of fiber have been experimented with, such as hollow core photonic crystal fiber, and double-cladding photonic crystal fiber [80]. Bao and Gu have compared double-clad fiber with double-clad photonic crystal fiber. They found that the double-clad fiber is better at efficiently utilizing the source laser power, while the double-clad photonic crystal fiber is more linear, and thus maintains polarization better by reducing self-phase modulation [81]. Nevertheless, advances have been made at developing a miniaturized two-photon fluorescence endoscope suitable for *in vivo* imaging due to compact optics, a reduction of multiple scattering, and a large field of view [76]–[78]. Flexible endoscopes for two-photon fluorescence imaging using a piezoelectric actuator for 2-D beam scanning have also been developed [79].

Two-photon microscopy has been used to obtain 3-D image volumes of normal, precancerous, and cancerous tissue biopsies of the hamster cheek pouch. Five statistically significant features were able to differentiate between the normal and the

precancerous or cancerous images, thus showing good potential for future clinical use [82]. Pulse shaping and phase modulation can be used for selective excitation of fluorescent probe molecules, as well as to compensate for unwanted phase distortions at the sample [83]. Multiphoton microscopy already extends past the maximum imaging depth of confocal microscopy, but further depths are always desirable. Oheim *et al.* discusses the tissue and instrument parameters which limit imaging depth in brain tissue, as well as how to make improvements to increase imaging depth [84]. To overcome the imaging limitations and deterioration of the point spread function due to sample aberrations and optical system imperfections, Marsh *et al.* has used a deformable mirror and automatic aberration correction based on fluorescence intensity feedback to extend the depth of imaging in two-photon microscopy [85]. With improvements such as these in the capabilities of multiphoton microscopy, it will no doubt become a more useful modality for clinical settings.

I. Endoscopic Imaging Modalities

Endoscopy, as a medical tool for observation and diagnosis, is straightforward in concept and has existed ever since 1807 when Phillip Bozzini used candlelight and mirrors to observe the canals of the human body. Numerous developments through the decades since then have taken the technology through the initial introduction of electric light for internal illumination all the way to flexible endoscopes using fiber optics, gradually improving the quality, noninvasiveness, and impact of endoscopic procedures.

Applications of endoscopy within the body are wide ranging, directed primarily in the upper and lower gastrointestinal tract, such as the esophagus and colon, but also in areas such as the bladder and even the brain. In general, current research is focused on producing higher quality endoscopic images by smaller devices able to reach previously inaccessible locations inside the body. All of this aims to be done with the primary goal of improving early diagnostic capabilities, while reducing costs and minimizing patient discomfort. It is hoped that endoscopy may be able to provide an easy method of mass screening at-risk patients for signs of cancer or precancerous tissue, including dysplasia and neoplasia. It is difficult to detect dysplasia using conventional endoscopic techniques, such as white light endoscopy. The gold standard of any endoscopic system is a histological analysis of a biopsied resection. Dysplasia can be detected through biopsy, but proper biopsy site need to be selected. For example, the Seattle Protocol for detecting early cancers in patients with the precondition of Barrett's esophagus recommends that four biopsies be taken in a quadrant pattern at 1 cm intervals [86], but there is a possibility that patterns such as these may still miss an important area. Biopsies impose a delay in diagnosis, are uncomfortable and intrusive for the patient, can be expensive, and may not even be optimal or necessary in contrast with less invasive techniques. To this end, methods such as the use of high resolution devices, narrow band imaging, infrared imaging, light induced fluorescence endoscopy, endoscopic optical coherence tomography, light scattering spectroscopy, and Raman spectroscopy, serve to image autofluorescence or subsurface tissue and reveal suspicious sites through image enhancement algorithms which may have otherwise gone unnoticed [87]. High resolution or magnification endoscopy seeks to obtain images with such fine detail that differences in cancer or noncancer can be clearly distinguished. Autofluorescence imaging is based on the fact that normal mucosa and adenoma or dysplastic mucosa exhibit different spectrums of autofluorescence that can be used to distinguish them. Narrow band imaging uses specific wavelengths of light which match absorption bands of hemoglobin, thus enhancing the contrast of micro vessels and other smaller tissue features. Infrared imaging can penetrate deeper tissue than visible light and therefore can visualize features such as blood vessels. Endo-cyto systems utilize magnification optics to visualize cells and cell nuclei when stained with a dye. Given the variety of tools available, a significant amount of research is focused on combining these methods of optical imaging within an endoscopic system. Naturally, this presents challenges due to the small size required by endoscopy: all components of the optical imaging system need to be contained in housing no bigger than a few millimeters in diameter. We will discuss some of the recent advancements made to various endoscopic modalities and present the challenges that each still face, along with some expectations for future work.

J. Endoscopic Fluorescence Imaging

The use of endoscopy in conjunction with tissue fluorescence has been shown to aid in cancer detection within the body and to provide better sensitivity than white light illumination alone. Fluorescence imaging helps to enhance the visual distinction between cancerous and healthy tissue, which may not always be visible or easy to delineate with conventional white light illumination. Cancerous tissue typically reveals itself by emitting an increased amount of fluorescent light compared to healthy tissue [88]; thus, these areas are best served as biopsy sites [89]. Depending on the fluorophore used, cancerous or healthy tissue fluorescence may also be manifested by different colors.

Despite the potential benefits of endoscopic fluorescence imaging and the high sensitivity it can provide, the technique is limited by low specificity, or, a large number of false positives. A clinical study of using fluorescence with endoscopy to image pharyngo-laryngeal cancer resulted in a sensitivity and specificity of 96% and 76%, respectively [90]. Likewise, endoscopic detection of oral cancers through fluorescence has a sensitivity in the range of 95%–100%, but a specificity of only 50%–60%. To combat this limitation, both the quantification of fluorescence intensity and the use of color channel intensity ratios (red/blue, red/green) were used to raise the sensitivity and specificity of detecting oral cancers to 95% and 97% respectively [91]. Using the fluorescence images to guide OCT imaging has also shown promise [92]. New fiber technology may even make it possible to utilize X-ray fluorescence in endoscopy. For results based on a tissue phantom, X-ray fluorescence image contrast was better than optical fluorescence imaging by an order of magnitude [93]. Nevertheless, refinement in endoscopic fluorescence imaging is a requirement before it can appear as a routine procedure.

K. Improvements in Endoscopic Distal Probe Hardware: Dynamically Changing Focal Depth and MEMS

The design of the endoscopic probe is an important consideration, because since the probe will be required to navigate through as small of an area as possible deep inside the body, space to hold optical components of the probe is limited. Still, notable advancements in distal probe hardware have been made. Conventionally, the optical configuration within the probe is fixed. Unmovable lenses result in a fixed focal depth, which may not be desirable, especially for endoscopic OCT applications. The ability to dynamically change the focal depth has therefore been demonstrated through use of a microfluidic hydraulic system [94] or pneumatic actuation [95] which deforms the curvature of a lens, thus modifying its focal depth. Another method involves using a gradient index (GRIN) lens rod, providing adjustments of focal range between 0 and 7.5 mm [96]. However, this method uses a rigid endoscope and therefore may not be useful for all types of endoscopy.

Another notable research area is that in the integration of microelecromechanical systems (MEMS) within the endoscopic probe to adjust mirrors and lenses to provide a wide range of optical scanning and direction adjustments [97]–[101]. By using mechanically movable mirrors within the probe itself, the direction of the scanning laser light can be reflected in multiple directions, thus increasing the scan range and scan angles of the probes without needing to move or rotate the catheter, which may be difficult especially when the probe is deep within the body along a contorted route. The illumination optical fiber itself can also be adjusted. The Scanning Fiber Endoscope (SFE) functions through use of a piezoelectric actuator. A cantilevered optical fiber is actuated in two dimensions to create a spiral pattern. This fiber serves as the illumination source to a small region of space along the path of the spiral. The backscattered illumination is then detected by a ring of additional fibers forming the outer shell of the endoscope, to detect the intensity value of the pixel on that particular point of the spiral. By varying the amplitude of the actuation, the field of view can be made wider or narrower, while maintaining good resolution [102]. The probe and tether can even be swallowed with a simple glass of water as a way to avoid patient sedation for the screening of Barrett's esophagus and esophageal cancer [103]. The piezoelectric effect has also been used to actuate mirrors to image at up to 25 fps [104]. A MEMS scanner and micromirror in [105] utilizes four electrothermal actuators to rotate and tilt the micromirror up to 45° and images in a circumferential scanning pattern. The micromirror discussed in [106] is dual-reflective, which likewise allows a full circumferential scan. Still, while MEMS and micromirror technologies are rapidly advancing, MEMS may be expensive and may be unreliable for repeated clinical use.

L. Other Notable Endoscopy Applications

In addition to the typical detection of cancer and precancer in common endoscopic areas such as the upper and lower gastrointestinal tract, endoscopy has also found applications in a variety of other locations in the body, with a number of different imaging objectives. Endoscopic imaging of the brain, known as neuroendoscopy, is subjected to narrower restrictions, but still has promise to permit imaging of transventricular regions or to perform endoscope-assisted microsurgery [107]. It has also been found that fluorescent endoscopy was possible even for deep-seated brain tumors such as in the third ventricle, with the use of a high powered laser at the specific excitation wavelength to ensure that fluorescent light would be visible [108].

It is now even possible to image blood flow in microvascular blood vessels less than 100 μm in diameter through the use of Endoscopic Doppler OCT (EDOCT) [109]. When tested for clinical feasibility, it was found that EDOCT imaging of small subsurface blood vessels revealed differences in microcirculation patterns of normal and diseased tissue, and therefore may be useful for diagnosis given further, more expansive testing [110]. Clearly, the limits of endoscopic imaging have yet to be reached and exciting new applications have yet to be applied.

M. Optical Coherence Tomography

OCT was invented in early 1990s but has recently emerged as a popular 3-D imaging technology for biomedical applications [111]–[113]. The relatively new modality makes use of the coherent properties of light [114]. In an OCT system, light with a low coherence length is divided into two parts. One part serves as a reference while the other is directed into the tissue. When light travels in tissue, it encounters an interface with a different refractive index and part of the light is reflected. This reflectance is subsequently mixed with the reference. Once the optical path length difference between the reference light and the reflected light is less than the coherence length, coherence occurs. By observing the coherence pattern and changing the optical path length of the reference light with a mirror, a cross section of the tissue can be rendered. With a sufficiently low coherence length, the resolution of OCT may reach a magnitude on the micrometer scale, hence it can disclose subtle changes in cancer tissue at a cellular level. OCT recovers the structure of interrogated tissue through a mechanism analogous to ultrasonic imaging. The latter modality sends sound into tissue which reflects when encountering an impedance varied interface. The resolution of OCT is much higher than ultrasonic imaging, but it cannot penetrate as far.

There are two types of broadly classified OCT systems: a single-point scanning based OCT system (Fig. 6) and a full field OCT system (Fig. 7). Images can be produced in time domain OCT mode through low coherence interferometry in which the reference path length is translated longitudinally in time. A fringe pattern is obtained when the path difference lies within the coherence length of the source. In frequency domain OCT (commonly known as FD-OCT), a broadband interference pattern is exploited in spectral dispersion. Spectrally separated detectors are encoded with optical frequency distribution onto a CCD or CMOS detector array so that the information about full depth is obtained in a single shot. Alternatively, in time-encoded frequency domain OCT (TEFD-OCT or Swept Source OCT), spectral dispersion on the detector is encoded in the time domain instead of with spatial separation [115]. The maximum reported imaging depths are between 1 and 3 mm [111]–[113], [115]–[118].

As OCT has emerged from interferometric methods, earlier investigations reported by Fujimoto *et al.* [117] were based

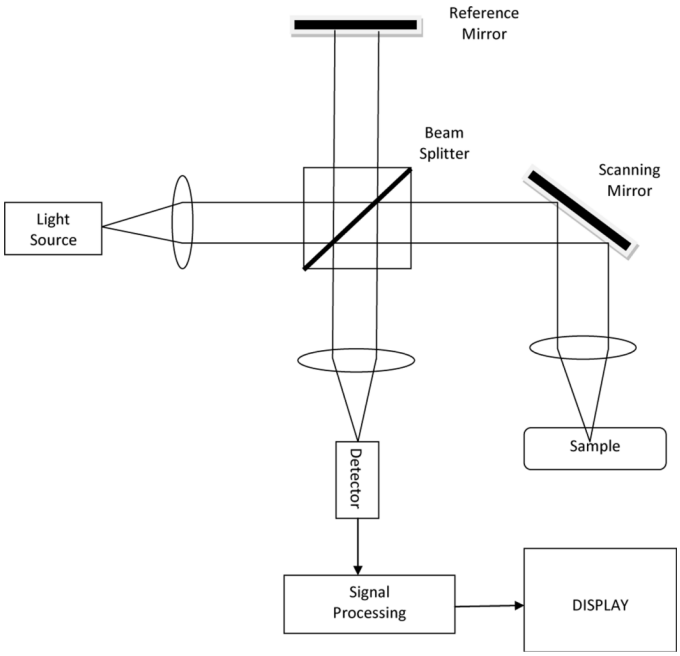

Fig. 6. Single-point scanning-based optical coherence tomography system.

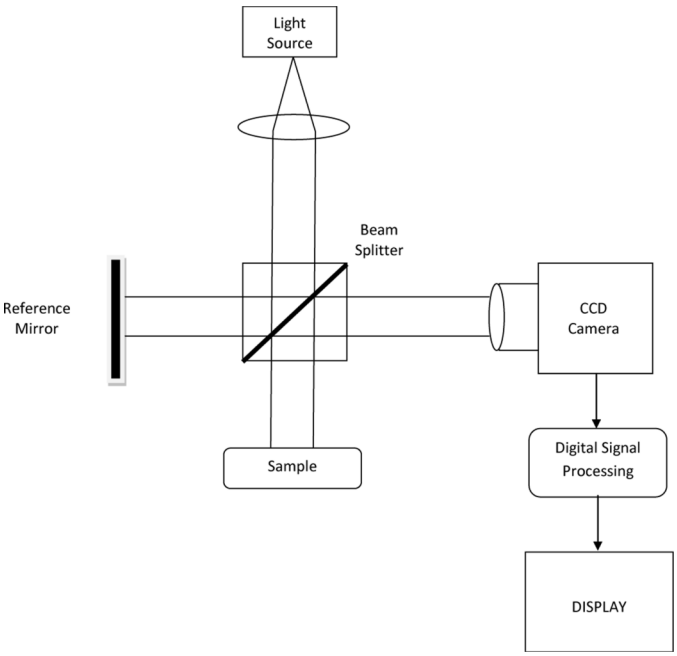

Fig. 7. Schematic diagram of full field optical coherence tomography system.

on femtosecond Michelson interferometry. Michelson interferometer based instrumentation has been most commonly investigated in OCT applications for retinal, skin, and vascular imaging [114], [119]–[131]. Recently, Kang *et al.* and others [132]–[141] have investigated common-path interferometer based OCT technologies. In common-path OCT, the sample and reference arms share a common path to allow a simpler design (Fig. 8). Kang *et al.* investigated a common-path interferometer based FD-OCT [134], [136] and used this for retinal imaging applications. Other common-path interferometer based approaches for time-domain OCT, using a free space interferometer, have also been demonstrated with limited success

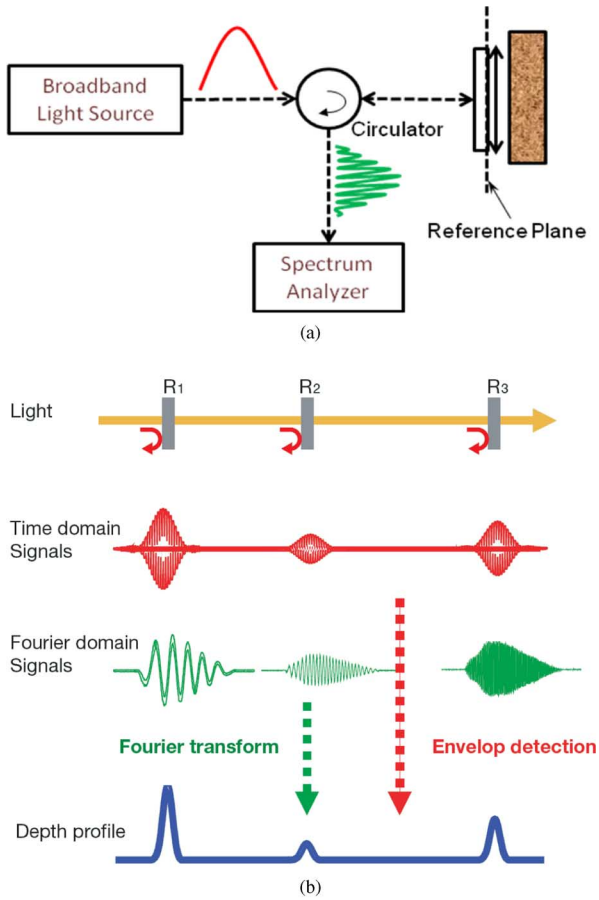

Fig. 8. (a) Schematic diagram of common-path OCT system and (b) time-domain and frequency-domain signal envelops (with permission from Jin Kang, John Hopkins University).

[141], [142]. Fiber optic-based technologies have been used for both frequency-domain and time-domain common-path OCT systems [132], [133], [135]–[139], [141]. Kang *et al.* [134] recently demonstrated the efficacy of fiber optic common-path OCT with a comparative assessment of existing endoscopic technologies. The Fourier domain common path optical coherence tomography has thus shown promising potential for intraocular surgical applications relevant to retinal surgery as the model application [134], [142], [143].

N. Endoscopic Optical Coherence Tomography

The combination of using OCT along with endoscopy is a relatively new field, emerging in 1996 as a potentially viable method of optical biopsy [144], [145]. The first clinical study occurred four years later, confirming that endoscopic optical coherence tomography (EOCT) images may be comparable to histological findings in esophageal, gastric, and colonic mucosa [125]. EOCT is capable of obtaining highly detailed images of multiple layers throughout the normal GI tract, including mucosa and submucosa [146], and these images have been verified to accurately match the histological structure of the GI tract [147]. EOCT is similar to endoscopic ultrasound (EUS) in that both use reflected waves to construct an image, however, EOCT uses near-infrared light while EUS uses sound. A comparison of the two technologies revealed that OCT images mucosa and submucosa layers of the GI wall with far superior resolution,

while catheter probe EUS penetrates to deeper layers (0.7–0.9 versus 10–20 mm) [148]. This is the advantage of EOCT: it may only penetrate to depths of around 1 mm, but image resolution is most commonly around 10 μm [149]. OCT imaging with even higher spatial resolutions than this is known as ultra high resolution OCT, and naturally provides finer detailed images. An *in vitro* study of Barrett's esophagus using an ultra high 1.1 μm resolution demonstrated improved visibility of architectural features and structural tissue recognition [150]. A later study used ultra high resolution OCT with an axial resolution of 5 μm in an *in vivo* study of 50 Barrett's esophagus patients and found that UHR OCT was a feasible method for the clinical setting, producing images with much better clarity and finer detail than standard OCT [151].

Despite promising research however, EOCT is still a technology in its clinical infancy. Demonstrations of EOCT have shown that it can potentially be useful to aid the diagnosis of cancerous and precancerous lesions within the gastrointestinal tract, but it remains to be seen whether this will translate well to widespread clinical usage. The full potential of EOCT may be initially limited due to the difficulty and inexperience of physicians to properly evaluate the resulting images. The question also remains if the technique will be viable in cost effectiveness once out of the prototyping stage. This question is especially relevant to the screening of patients with Barrett's esophagus; while this group is at high risk for esophageal cancer, only an estimated 0.5% of those with the condition develop cancer per year [87]. Any widespread screening method therefore needs to be quick, accurate, and inexpensive.

A number of efforts have been made to test the viability of EOCT in a clinical setting, though on a small scale. In a double blind study of 33 patients, EOCT returned a diagnostic accuracy averaged among four endoscopists of 78% in detecting dysplasia in Barrett's esophagus compared to a biopsy evaluation [152]. The results of the study thus show that while EOCT could be used for intelligently targeting biopsy sites, improvements in accuracy are still needed for EOCT to be used exclusively in a clinical setting. Another study hoped to improve detection of dysplasia in Barrett's esophagus in 106 images from 13 patients through the use of a computer aided diagnosis algorithm. However, when compared with histology, the resulting sensitivity, specificity, and accuracy of 82%, 74% and 83% respectively, showed potential but still necessitate further improvements [153]. A much larger study was undertaken more recently, comprised of 554 patients, to detect either early urinary bladder or gastrointestinal tract cancers. The respective sensitivity and specificity were reported as 71%–85% and 68% for neoplasia detection in Barrett's esophagus, 85% and 68% for bladder carcinoma, and 92% and 84% for colon dysplasia [154]. The larger clinical group is a good step, as EOCT needs validation from a larger number of patients, but accuracy rates can still be improved.

O. Diffuse Reflectance and Transillumination Imaging

Diffuse reflectance images are formed by backscattered diffused light (see Fig. 9). These images represent composite information about the absorption and scattering by different chromophores and biological structures in the medium. Although the raw images produced may be useful and may carry important diagnostic information, more significant information can be derived from three dimensional reconstruction of the biological medium from multispectral diffuse reflectance measurements.

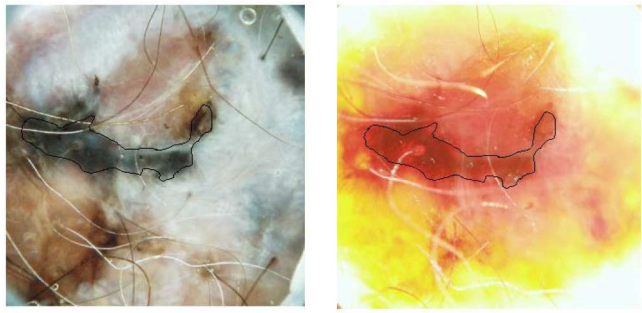

(a) (b)

Fig. 9. Surface reflectance based epi-illuminance light microscopy (ELM) image (a) of malignant melanoma skin lesion with a backscattered diffuse reflectance based transillumination image (b) obtained by the Nevoscope [155], [156]. Increased absorption due to larger blood volume around the outlined lesions boundary is evident.

To obtain a 3-D reconstruction of the biological medium from diffuse reflectance measurements, a forward model is required to relate the measurement to the optical properties of investigated tissue. Regardless of what kind of imaging geometry we are using, an optical system may be described as

$$M = F(x) \tag{16}$$

where M is the measurement, F is a forward model, and x is a distribution of unknown optical properties. Given a reasonable initial guess x_0 of the background optical properties, (16) can be extended to

$$M = F(x_0) + F'(x_0)(x - x_0) + \frac{1}{2}F''(x_0)(x - x_0) + \cdots \tag{17}$$

where F' and F'' are first-order and second-order Frechet derivatives, respectively.

If we let $\Delta M^{cal} = M - F(x_0)$ and $\Delta x = x - x_0$, (17) may be rearranged as

$$\Delta M^{cal} = F'\Delta x + \frac{1}{2}F''\Delta x + \cdots. \tag{18}$$

The discrete form of the above equation can be expressed as an expansion such that

$$\Delta \vec{M}^{cal} = J\Delta\vec{x} + \frac{1}{2}H\Delta\vec{x} + \cdots \tag{19}$$

where J is the Jacobian matrix, H is the Hessian matrix, $\Delta\vec{M}^{cal}$ is the measurement vector, and $\Delta\vec{x}$ is the vector that gives the variations from the background $\vec{x}_0$.

Neglecting the higher order terms in (19), a linear system can be represented by the Jacobian matrix as

$$\Delta \vec{M}^{cal} = J\Delta\vec{x}. \tag{20}$$

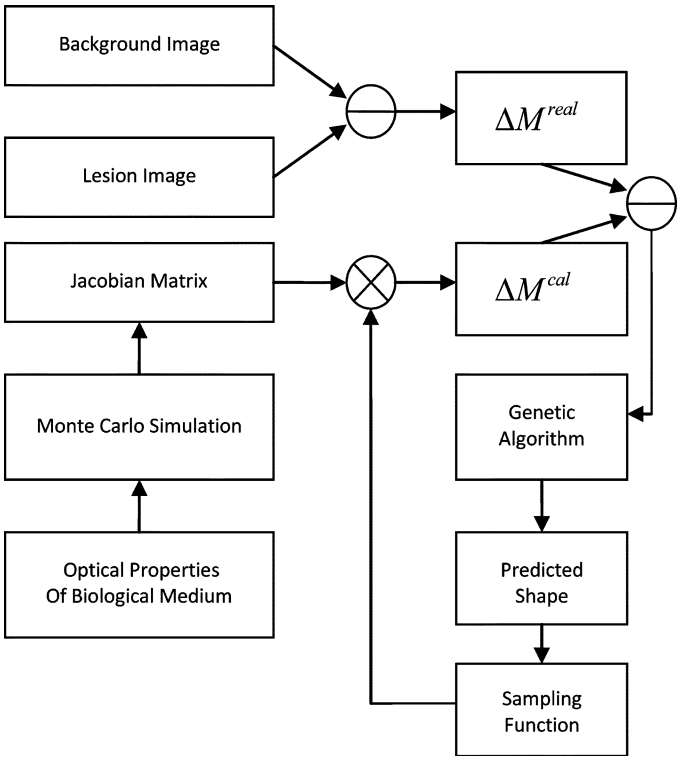

Fig. 10. General schematic of 3-D reconstruction from multispectral diffuse reflectance images [157].

The formulation in terms of (20) leads to linear optical tomography which is also known as difference imaging. Two measurements are taken; one is for background tissue (that is, x_0) and one is for abnormal tissue (that is, unknown x). The difference between these measurements is then fed into the reconstruction algorithm to obtain the optical properties. Since this is an extremely ill-posed inverse solution problem, *a priori* shape information can be used to find a reasonable solution as shown by several investigators [23], [157]–[160]. A generalized lesion reconstruction method from multispectral diffuse reflectance using shape based information is schematically shown in Fig. 10. This method uses a Monte Carlo simulation based forward model to reconstruct the lesion in the biological medium using a genetic algorithm based optimization to weight the contribution from acquired multispectral diffuse reflectance measurements.

Dhawan *et al.* developed a novel optical imaging system, the Nevoscope, that uses transillumination to provide images of skin lesions showing subsurface pigmentation as well as vascular architecture based blood volume information [155]. Their paper presents a Nevoscope transillumination method to acquire this information and compare its performance to the epiluminescence imaging method for its ability to measure vascular information for the characterization of skin lesions.

Patwardhan *et al.* then used the Nevoscope and transillumination method as a basis for simulating the skin lesion volume [161]. Three-dimensional, voxel based, and wavelength dependent skin lesion models were developed and simulated using Monte Carlo techniques. The thickness of the lesion was characterized and based on correlation analysis between diffuse reflectance images using specific optimal wavelengths selected for multispectral imaging of skin lesions using the Nevoscope. Optical properties of tissue reported by various researchers were compiled together to form a voxel library. The tissue models used in the simulations were developed using the voxel library which offered flexibility in updating the optical properties and adding new media types into the models, independent of the Monte Carlo simulation code [161]. The simulated multispectral transillumination images acquired with the Nevoscope were fed into a genetic algorithm-based optimization program where the optical properties were reconstructed in terms of measurements at multiple wavelengths. The distribution of melanin and blood was subsequently calculated by Wang and Dhawan [157]. Results of the reconstruction of melanin and blood parts were presented for simulated lesions using multispectral wavelengths at 580 nm and 800 nm. Thus, useful results can be obtained from the analysis of diffuse reflectance and transillumination images.

P. Fluorescence Diffused Optical Tomography (FDOT)

Three-dimensional image reconstruction in fluorescence diffuse optical tomography (FDOT) is a very challenging problem due to the scattered attenuation of limited emission in the tissue as well as uncertainties associated with mapping of the illumination source on the detector plane [162]–[164]. Images recorded in the detector plane suffer from poor signal-to-noise ratio and are sensitive to the whole-tissue volume effect. Reconstruction of emission distributions from FDOT data suffer from underdetermined ill-posed imaging conditions. Mathematical models based on radiative transport (e.g., Monte Carlo techniques), the diffusion equation, and iterative optimization methods have been used for FDOT image reconstruction [165]–[178]. Forward models of photon propagation for diffuse optical tomography are discussed in [168]–[171]. The inverse solutions have been investigated using direct inversion methods utilizing Green's functions as well as iterative optimization methods [168]–[178]. Patwardhan *et al.* investigated FDOT image reconstruction using Born's approximation with ratiometric measurements [40]. The fluorophore concentration was reconstructed by inverting ratiometric data derived from the intensities of the excitation and fluorescence light measured on the detector plane for each source position. Following the normalized Born approach [166], formulation of the ratiometric fluorescence and excitation measurements was modeled with the measurement vector Y, through mapping the unknown source distribution X with an imaging matrix A as

$$[Y] = [A][X] \tag{21}$$

where the matrix elements were defined as [40]

$$y_i = \left[\frac{\Phi(\mathbf{r}_{s(i)}, \mathbf{r}_{d(i)}, \lambda_{emi}) - \theta_f \Phi_o(\mathbf{r}_{s(i)}, \mathbf{r}_{d(i),} \lambda_{exc})}{\Phi_o(\mathbf{r}_{s(i)}, \mathbf{r}_{d(i),} \lambda_{exc})}\right] \tag{22}$$

$$A_{i,j} = -\frac{S_o v h^3}{D_o} \frac{G(\mathbf{r}_{s(i)}, \mathbf{r}_j, \lambda_{exc}) G(\mathbf{r}_j, \mathbf{r}_{d(i)}, \lambda_{emi})}{G(\mathbf{r}_{s(i)}, \mathbf{r}_{d(i)}, \lambda_{exc})} \tag{23}$$

$$x_j = \partial N_j. \tag{24}$$

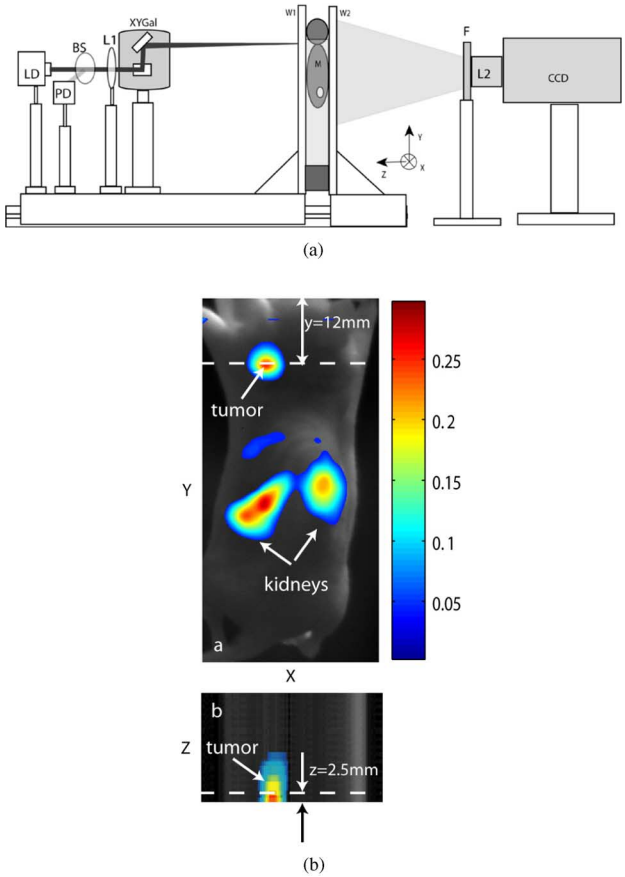

Fig. 11. (a) Fluorescence tomography system. Mouse subject is suspended and held in light compression between two movable windows (W1 and W2). Light from a laser diode at 785 nm (LD) is collimated and passes through a 95/5 beam splitter (BS). Reference photodiode (PD) collects 5% of the beam. Main 95% beam passes through lens (L1) into a XY galvo scanning system (XYGal). Mirror pair scans the beam onto the illumination window (W1) of the imaging tank. Light emitted from W2 is detected by an EMCCD via a filter (F1) and lens system (L2) [40]. (b) Representative slices from 3-D tomographic reconstruction of a nude mouse with a subcutaneous breast-specific cancer, xenograft MDA MD 361. Top: XY slice parallel to the detector plane at a depth of $Z = 2.5$ mm. Bottom: XZ slice extending from source plane to detector plane at $y = 12$ mm. Taken with permission from [40].

In (22), $\Phi(\mathbf{r}_{s(i)}, \mathbf{r}_{d(i)}, \lambda_{exc})$ represents the fluence at excitation wavelength λ_{exc}. The variables $\mathbf{r}_{s(i)}$ and $\mathbf{r}_{d(i)}$ are the positions of the ith source-detector pair locations (facing each other). Similarly, the fluence at the emission wavelength λ_{emi} is written as $\Phi(\mathbf{r}_{s(i)}, \mathbf{r}_{d(i)}, \lambda_{emi})$. G is a two point Greens function, and image voxel x_j has a concentration differential ∂N_j and position r_j. These equations can then be numerically solved using a conjugate gradient, singular value decomposition, or algebraic reconstruction technique with appropriate constraints and regularization method [162], [167]–[174]. Fig. 11(b) shows 3-D reconstructed FDOT images from a nude mouse with a subcutaneous breast-specific cancer lesion using the experimental setup shown in Fig. 11(a).

Several researchers have investigated a variety of different dyes in FDOT imaging and 3-D reconstruction for tumor analysis through molecular and blood flow imaging, such as pharmacokinetics of ICG and HPPH-car, as well as hydrophilic cyanine dyes [178]–[180]. Fluorescence enhanced optical imaging methods for breast cancer was demonstrated for clinical potential in diagnostic radiology [181]. Zagaynova *et al.* has used hybrid OCT and fluorescence imaging methods for detection and characterization of bladder neoplasia and GI cancer [154], [182]–[184]. Corlu *et al.* also recently examined the use of FDOT for *in vivo* imaging of breast cancer with the fluorophore Indocyanine Green (ICG). Fluorescence excitation and detection was accomplished using 786-nm laser sources which were then spectrally filtered for CCD detection. Phantom and *in vivo* images were reconstructed for ICG fluorescence and were well correlated with MRI images of the breast tumors [185]. More applications in molecular imaging through fluorescence with NIR imaging are discussed by Ntziachristos *et al.* [162].

Q. Optical Transillumination Imaging

Transillumination, also known as shadowgram optical imaging or diaphanography, was first used by Cutler in 1929 to examine pathology in the breast with the unaided eye [186]. Transillumination was initially surpassed by the superiority of X-ray technology, but later evolved to be a major application of visible light in medicine, particularly in aiding the early detection and diagnosis of breast cancer [186]–[198].

Since assessing breast cancer risk with optical transillumination would avoid the need for ionized radiation through X-ray mammography, it could safely be applied more frequently to women of all ages. The parenchymal tissue density pattern is a good indicator of future breast cancer risk and is typically obtained through mammography. As an alternative, chromophore compositions and morphology of the breast tissue, as observed though transillumination, has been found to identify women with high parenchymal density. This method may therefore provide the same odds ratio for breast cancer risk as can traditional mammography, thus showing that it may offer an alternative to radiation screening [199], [200].

While transillumination is often performed using white visible light, infrared and even ultraviolet light are commonly used to observe interesting tissue characteristics which may not be apparent under the visible spectrum [201]. The recent widespread availability of near-infrared (NIR) lasers and CCDs has led to further research in optical transillumination modalities with infrared light, particularly in the last two decades [202]. For example, in 1980 Ohlsson reported on a technique using near-infrared sensitive film to photograph the transilluminated breast. Other research into the optical transmission characteristics of the breast has involved an NIR dual wavelength pulsed light source [191], [203]. Using a 1250-nm laser for transillumination, differences in contrast and resolution were observed between normal breast tissue and cancerous breast tissue. This higher range of wavelength was found to result in enhanced contrast, higher resolution, and deeper penetration than shorter wavelengths. Specifically, at 1225 nm, images showed clear distinction between fatty and fibrous human breast tissues [204].

A time-resolved technique has also been used to make possible simultaneous, multispectral transillumination of a breast phantom, which could be used for measuring optical properties of tissue [205]. With this time resolved technique, it has been found that depending on the temporal probability density function of the first arriving photon, conclusions can be made about the medium through which the photons were transilluminated [206].

However, the primary difficulty with optical transillumination is strong scattering in the biological tissue due to its diffuse nature. Thus, spatial resolution and reproducibility of reconstructed images are significant challenges in optical transillumination, due to the ill-posed and underdetermined nature of reconstruction. A number of approaches has been investigated to estimate the point spread function of optical transillumination imaging so that the final reconstructed images can be processed properly to improve image quality and thereby improve the diagnosis of breast tumors. One approach involves the use of various time-dependent point spread functions to analyze the diffusive and absorptive contrasts and then deconvolve the time-resolved transilluminated images [207]. Extraction of the near-axis scattered light component has been used to help suppress the scattering effect in transillumination imaging [208]. Using the time of flight information can also improve spatial resolution of images [209], [210]. The Coherent Detection Imaging (CDI) method has been used for transillumination optical computed tomography and has been found to be appropriate for CT reconstruction [211]. Using the radiative transfer equation, Moon *et al.* found the mathematical limits of photonic transport and how this relates to the theoretical best point spread function achievable [212]. The point spread function directly influences the maximum spatial resolution, which can be as low as 2 mm with ideal signal-to-noise ratio and detector gate times of around 10 ps [213].

Transillumination is not only used just for the breast. Applications of the technique extend also into dental imaging, with the use of fiber optic transillumination (FOTI) to monitor dental caries [214]. Using first and second moments as well as wavelet decomposition of FOTI images, changes in tooth decay over time can be reliably identified and monitored, which may not have been detected in the spatial domain [215]. Early detection of these dental caries in the interproximal contact sites between teeth was also demonstrated with an infrared transillumination system [216]. Other locations of the body where NIR transillumination imaging has been studied include tissues in the forearm and thumb [217].

Functional transillumination imaging is also of key interest. Voltage sensitive dyes have promising applications for visualizing 3-D cardiac activity with transillumination. Simulations have been performed for detecting scroll waves in the ventricular wall [218], [219]. Inhaled hyperoxic and hypercarbic gases were used as contrast agents to change the concentration of HbO_2 and Hb in blood, thereby increasing the visibility of atypical tumor vasculature after transillumination [220]. Hybrid diffusion models of diffuse optical tomography have also recently been studied for diagnostic applications [221]–[227]. For example, phase contrast diffuse optical tomography of the breast may be helpful in differentiating malignant and benign lesions [221]. Diffuse optical tomography may also be used for functional imaging of the brain to characterize epileptic lesions [224], [225].

IV. Photoacoustic Imaging: Emerging Technology

Photoacoustic imaging is a fast emerging technology that utilizes the acoustic waves from thermal expansion of an absorbing object, such as a tumor, pigmented lesion, or blood vessel, caused by the absorption of light photons. In biomedical imaging applications, light from a short pulsed laser scatters inside the target object producing heat. The temperature is raised by a fraction of a degree, causing thermal expansion. The thermoelastic effect generates pressure transients which exactly represent the absorbing structures. These pressure transients produce ultrasonic waves that propagate to the tissue surface and are detected by an ultrasound sensor. The photoacoustic imaging methods are also known as optoacoustics, laser induced ultrasound, or thermoacoustics imaging, and have been investigated for imaging lesions of the breast, skin and vascular tissues [228]–[233]. A nice overview of the photoacoustic effect and imaging methods is presented in a dissertation by Niederhauser [234] and also in a tutorial paper by Wang [235]. The spatial resolution of photoacoustic imaging depends on the photoacoustic emission phase. As described in [235], strong optical scattering in biological tissue causes shallow imaging depth and low spatial resolution. Since ultrasound scattering is much weaker than optical scattering, the resulting ultrasound signal from photoacoustic imaging provides better resolution than optical diffuse imaging methods. Figs. 12 and 13 show a photoacoustic microscopy (PAM) system developed by Wang *et al.* and Zhang *et al.* to produce high contrast high resolution functional images of the skin [235], [236].

Photoacoustic imaging has also been extended to three dimensions with photoacoustic tomography (PAT) using the modified back projection method [237]–[240], the regularized Newton method, and iterative algebraic reconstruction-based methods [241]–[243]. PAT images contain some blurring effects which require appropriate filtering to improve image quality. Regularization methods as well as *a posteriori* filtering methods have been investigated [240]–[243]. Quantitative photoacoustic tomography-based radiative transfer equation has been investigated by Yuan and Jiang [244], [245], who studied the recovery of the physiological and optical properties of biological tissue including the brain for characterization of epileptic lesions [245]–[247]. Fig. 14 shows an imaging setup for PAT developed by Wang *et al.* [239]. Photoacoustic axial images of a hemodynamic response of a rat brain as obtained from PAT by Wang *et al.* [239] are shown in Fig. 15. A significant increase in the optical absorptions at the positions of blood vessels in the cerebral cortex in hypoxia is believed to be due to an increase in cerebral blood flow.

V. Discussion and Concluding Remarks

In this paper, we have presented an overview of many of the important optical imaging technologies currently being researched, as well as an overview of light propagation modeling in a biological turbid medium for the simulation of photon interaction in tissue. Other reviews on optical imaging methods are nicely discussed in the literature [248]–[250], and for further technical and mathematical details about these methods, we refer the reader to recent in-depth books on the subject matter [3], [251]–[253]. In this review, however, we have presented an overview of the technologies available and emphasized the current and future work being performed by various research

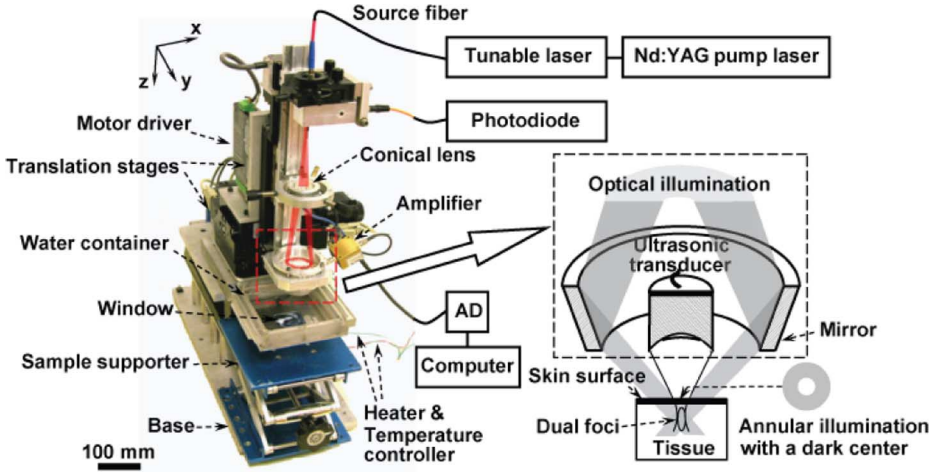

Fig. 12. Experimental fPAM system. Components within dashed box in photograph are mechanically translated along X–Y plane with bottom of mirror and ultrasonic transducer immersed in water. Window at the bottom of water container is sealed with optically and ultrasonically transparent disposable polyethylene membrane (thickness, 0.044 mm). After commercially available ultrasound gel is applied to the region of interest on sample for acoustic coupling, sample is placed between water container and sample supporter for imaging (taken from [236] with permission).

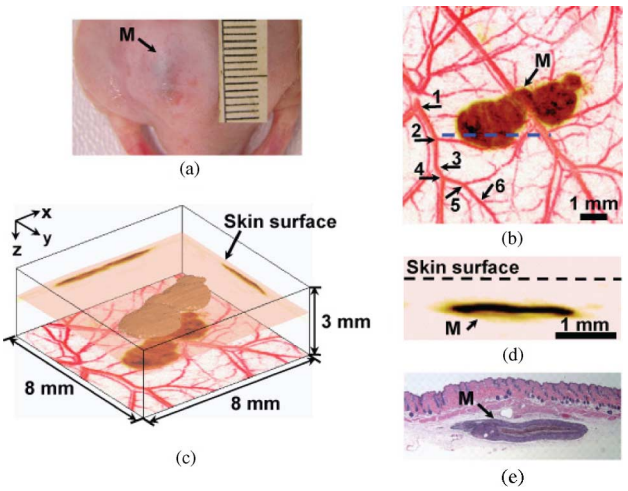

Fig. 13. *In vivo* imaging of a subcutaneously inoculated B16-melanoma in an immuno-compromised nude mouse using fPAM at 584 and 764 nm. (a) Photograph of melanoma. (b) Composite of two maximum amplitude projection (MAP) images projected along Z axis, where MAP image is formed by projecting maximum photoacoustic amplitudes along a direction to its orthogonal plane. Here, blood vessels are pseudocolored red in 584-nm image and melanoma is pseudo-colored brown in 764-nm image. As many as six orders of vessel branching can be observed in image as indicated by numbers 1–6. (c) Three-dimensional rendering of melanoma from data acquired at 764 nm. Two MAP images at this wavelength projected along X and Y axes are shown on two side walls, respectively. Composite image shown in (a) is redrawn at bottom. Top surface of tumor is 0.32 mm below skin surface, and thickness of melanoma is 0.3 mm. (d) Enlarged cross-sectional (B-scan) image of melanoma parallel with Z-X plane at location marked with dashed line in (a). (e) Hematoxylinand-eosin (HE) stained section at same marked location. M denotes melanoma (taken from [236] with permission).

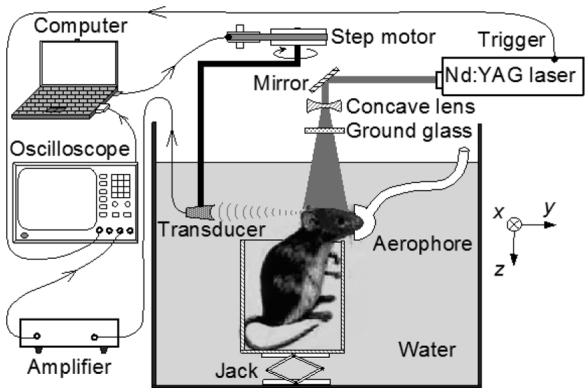

Fig. 14. Imaging setup for PAT developed by Wang *et al.* (taken from [239] with permission).

groups. More importantly, we have focused on the current clinical significance of these optical imaging methods for patient benefits.

Optical imaging modalities have a common advantage of low infrastructure costs while being portable and capable of functional imaging at tissue, cellular, and even molecular levels. Among all of the optical imaging modalities, endoscopy has been the most successful so far. Other modalities, such as fluorescence microscopy, confocal microcopy, diffuse reflectance, optical coherence tomography, and transillumination, have shown significant potential in diagnostic applications but still have to prove their high sensitivity and specificity in specific clinical practice. For example, an official technology assessment by the American Academy of Ophthalmology on confocal microscopy, performed in 2004, found that confocal microscopy had the greatest potential in facilitating the diagnosis of infectous keratitis and refractive surgery, but so far there had been no studies to support its use in managing eye disorders and little by way of clinical applications and support of its use as an adjunctive diagnosis [254]. Likewise, a feasibility study was conducted in [255] to determine the usefulness of reflectance-type laser scanning confocal microscopy compared to histological images of gastrointestinal neoplastic lesions. Differences in nuclei shape were seen between malignant and nonmalignant cells for some, but not all, of the cases. Thus, only with further improvement would confocal microscopy be able to aid immediate diagnosis without any other corroborating methodology.

Confocal microscopy can play a critical role in the understanding of tissue structure and disease and has demonstrated

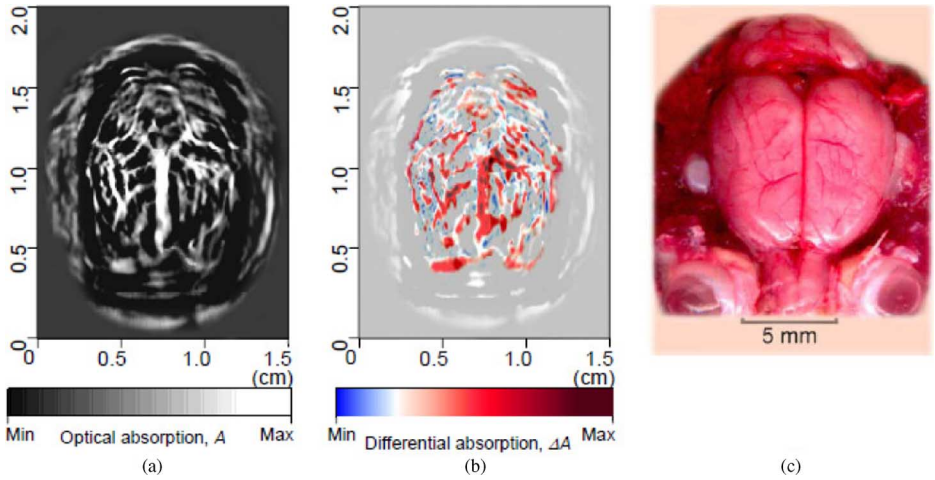

Fig. 15. Noninvasive PAT of cerebral hemodynamic responses to alteration from hyperoxia to hypoxia. (a) Noninvasive PAT image of vascular distribution in rat cerebral cortex, which was acquired with skin and skull intact. (b) Noninvasive functional PAT image of cerebral hemodynamic responses to altering inspired gas from 100% O_2 to 5% O_2 acquired with skin and skull intact. This functional map is superimposed on image of vascular distribution shown in (a). (c) Open-skull photograph of rat cortical surface obtained after PAT experiment (taken from [239] with permission).

the differentiation between normal and abnormal tissue for cancer diagnosis. However, as it is still a relatively new technology, true clinical application has yet to be established. This technique still needs to be assessed in more expansive clinical trials to validate its diagnostic potential. Improvements could also be made to increase the overall accuracy of confocal imaging in order to improve its reliability as a clinical tool.

Likewise, there have been many interesting investigations and applications of multiphoton microscopy in biomedical imaging, but improvements and refinements in instrumentation will still play a critical role in future. Miniaturizations of the optical and fiber components are of utmost importance in order to reliably utilize the multiphoton technique *in vivo*. Better temporal resolution will allow finer observation of cellular behavior. Furthermore, improvements in the technological aspects will hopefully enable multiphoton and two-photon microscopy to play a bigger role in clinical analysis and diagnosis of cancerous and precancerous tissue. Several methods and techniques for improving endoscopic imaging have been heavily investigated recently. By integrating imaging methods such as OCT and fluorescence with new generation endoscopes, the potential for better *in vivo* diagnosis of cancers is rapidly increasing. All of these developments help make the move toward efficient optical biopsy. Such endoscope systems have already been constructed and the theory and feasibility have been demonstrated [256]. However, despite the excitement surrounding these integrated methods and the wide variety of currently demonstrated applications, the extension of these research prototype technologies into mainstream clinical usage is not yet ready. Some even have warned that clinicians should not currently use these technologies to guide their decisions about patients until more data has been obtained about how best to use these methods to screen and survey patients [257]. Many small scale clinical trials have been reported with a good amount of success, but the applicability and feasibility of these endoscopic techniques still need to be tested and verified in large scale trials. Large scale trials will serve two functions: first, to validate the diagnostic accuracy over a wider range of potentially non-ideal candidates, and second, to evaluate their cost effectiveness.

Given the current difficulties with individual methods, it is generally agreed that rather than any one method evolving sufficiently to become a standard, a combined approach involving two or more methods will be the likely end result for clinical endoscopic procedures. This approach already has support from the literature, as improved diagnostic accuracy has been demonstrated in endoscopic systems by combining simultaneous fluorescence imaging with OCT to detect early bladder cancer [258], fluorescence imaging with spectroscopy [259], and fluorescence image guided OCT [92]. Another hybrid approach uses video endoscopy with a mode selector, which can switch between white light imaging, autofluorescence imaging, narrow band imaging, and infrared imaging. The mode selector automatically adjusts the filters and color separators needed for correct functionality [260].

It is logical that integrating more than one imaging method will improve the chances that a malignant lesion will be indentified early enough to excise the lesion and save the life of the patient. Future work is expected to focus on developing a reliable and standardized system for clinical applications. Other future research may involve grading degrees of dysplasia, reducing false positives, and improving endoscopic hardware to image smaller inaccessible ducts of the body and to enable endoscopic resection and ablation.

Diffuse optical tomography too has emerged as a promising functional imaging modality, as it can provide quantitative and dynamic tomographic imaging of neural brain tissue [261]. Changes in local hemodynamic response have been recorded through transillumination imaging, diffuse reflectance tomography and photoacoustic imaging with clinical applications to brain imaging and detection of breast and skin cancers [155], [157], [262], [263]. A series of dynamic 2-D images have been obtained to delineate the time course of concentration changes of oxyhemoglobin, deoxyhemoglobin, and total hemoglobin in the rat brain during seizure onset [224], [261].

As detector technology continues to improve, the sensitivity of optical imaging modalities will continue to progress, as will the development of cost-effective portable imaging technologies for structural and functional imaging at tissue, cellular, and molecular levels for clinical diagnostic and therapeutic applications. Such developments will also be benefited through better understanding and more accurate models of photon propagation in a turbid biological medium for reproducible improvements in tomographic 3-D image reconstructions. Furthermore, hybrid imaging methods such photoacoustic imaging technologies demonstrate a realistic potential towards future functional imaging with clinical significance.

ACKNOWLEDGMENT

The authors would like to thank Dr. L. Wang, Dr. J. Kang, and Dr. S. Patwardhan for providing some of the images included in this paper.

REFERENCES

[1] 2009 [Online]. Available: http://www.molecularstation.com/molecular-biology-images/

[2] M. Born and E. Wolf, *Principles of Optics: Electromagnetic Theory of Propagation, Interference and Diffraction of Light*, 7th ed. Oxford, U.K.: Cambridge Univ. Press, 1999.

[3] L. V. Wang and H.-i. Wu, *Biomedical Optics: Principles and Imaging*. Hoboken, NJ: Wiley, 2007.

[4] C. Bohren and D. Huffman, *Absorption and Scattering of Light by Small Particles*. New York: Wiley-Interscience, 1983.

[5] A. Ishimaru, *Wave Propagation and Scattering in Random Media*. New York: IEEE Press, 1999.

[6] R. R. Anderson and J. A. Parrish, "The optics of human skin," *J. Investigative Dermatol.*, vol. 77, no. 1, pp. 13–19, 1981.

[7] A. N. Bashkatov *et al.*, "Optical properties of human skin, subcutaneous and mucous tissues in the wavelength range from 400 to 2000 nm," *J. Phys. D: Appl. Phys.*, vol. 38, no. 15, pp. 2543–2555, 2005.

[8] M. J. C. Van Gemert *et al.*, "Skin optics," *IEEE Trans. Biomed. Eng.*, vol. 36, no. 10, pp. 1146–1154, Oct. 1989.

[9] I. V. Meglinski and S. J. Matcher, "Quantitative assessment of skin layers absorption and skin reflectance spectra simulation in the visible and near-infrared spectral regions," *Physiol. Measure.*, vol. 23, no. 4, pp. 741–753, 2002.

[10] A. D. Kim, "Transport theory for light propagation in biological tissue," *J. Opt. Soc. Amer. A: Optics Image Science, and Vision*, vol. 21, no. 5, pp. 820–827, 2004.

[11] S. Chandrasekhar, *Radiative Transfer*. New York: Dover, 1960.

[12] A. P. Dhawan, R. Gordon, and R. M. Rangayyan, "Nevoscopy: Three-dimensional computed tomography of nevi and melanomas *in situ* by transillumination," *IEEE Trans. Med. Imaging*, vol. MI-3, pp. 54–61, 1984.

[13] C. L. Leakeas and E. W. Larsen, "Generalized Fokker–Planck approximations of particle transport with highly forward-peaked scattering," *Nuclear Sci. Eng.*, vol. 137, no. 3, pp. 236–250, 2001.

[14] J. E. Morel, "An improved Fokker–Planck angular differencing scheme," *Nucl. Sci. Eng.*, vol. 89, no. 2, pp. 131–136, 1985.

[15] J. M. Schmitt *et al.*, "Multilayer model of photon diffusion in skin," *J. Opt. Soc. Amer. A, Optics Image Sci.*, vol. 7, no. 11, pp. 2141–2153, 1990.

[16] A. Ishimaru, *Wave Propagation and Scattering in Random Media*. New York: Academic, 1978.

[17] S. T. Flock *et al.*, "Monte Carlo modeling of light propagation in highly scattering tissues -I: Model predictions and comparison with diffusion theory," *IEEE Trans. Biomed. Eng.*, vol. 36, no. 10, pp. 1162–1168, Oct. 1989.

[18] L. Wang, S. L. Jacques, and L. Zheng, "MCML—Monte Carlo modeling of light transport in multi-layered tissues," *Computer Methods Programs Biomedicine*, vol. 47, no. 2, pp. 131–146, 1995.

[19] S. A. Prahl *et al.*, "A Monte Carlo model of light propagation in tissue," *SPIE Inst. Ser.*, vol. 5, no. 5, pp. 102–111, 1989.

[20] C. M. Gardner and A. J. Welch, "Monte Carlo simulation of light transport in tissue: Unscattered absorption events," *Appl. Opt.*, vol. 33, no. 13, pp. 2743–2745, 1994.

[21] L. Wang and S. L. Jacques, *Monte Carlo Modeling of Light Transport in Multi-layered Tissues in Standard C*. Houston, TX: Univ. Texas, M.D. Anderson Cancer Centre, 1992.

[22] M. Keijzer *et al.*, "Light distributions in artery tissue: Monte Carlo simulations for finite-diameter laser beams," *Lasers Surgery Medicine*, vol. 9, no. 2, pp. 148–154, 1989.

[23] T. J. Pfefer *et al.*, "Adaptable three-dimensional Monte Carlo modeling of imaged blood vessels in skin," *Laser-Tissue Interaction VIII.*, pp. 2–13.

[24] I. G. Zubal and C. R. Harrell, "Voxel based Monte Carlo calculations of nuclear medicine images and applied variance reduction techniques," *Image Vision Computing*, vol. 10, no. 6, pp. 342–348, 1992.

[25] R. P. Hemenger, "Optical properties of turbid media with specularly reflecting boundaries: Applications to biological problems," *Appl. Opt.*, vol. 16, no. 7, pp. 2007–2012, 1977.

[26] H. Van de Hulst, *Multiple Light Scattering: Tables, Formulas, and Applications*. New York: Academic, 1980.

[27] I. D. Miller and A. R. Veitch, "Optical modelling of light distributions in skin tissue following laser irradiation," *Lasers Surg. Med.*, vol. 13, no. 5, pp. 565–571, 1993.

[28] L. Reynolds, C. Johnson, and A. Ishimaru, "Diffuse reflectance from a finite blood medium: Applications to the modeling of fiber optic catheters," *Appl. Opt.*, vol. 15, no. 9, pp. 2059–2067, 1976.

[29] W. S. Snyder *et al.*, "Estimates of absorbed fractions for monoenergetic photon sources uniformly distributed in various organs of a heterogeneous phantom," *J. Nucl. Med.*, pp. Suppl 3:7–52, Aug. 1969.

[30] L. G. Henyey and J. L. Greenstein, "Diffuse radiation in the galaxy," *Astrophys. J.*, vol. 93, pp. 70–83, 1941.

[31] E. Hecht and A. Zajac, *Optics*, 2nd ed. Reading, MA: Addison-Wesley, 1987.

[32] L. L. Carter and E. D. Cashwell, "Particle transport simulation with the Monte Carlo method," U.S. Energy Res. Development Admin., TID-26607, 1975.

[33] J. S. Hendricks and T. E. Booth, "MCNP variance reduction overview," *Lect. Notes Phys.*, vol. 240, pp. 83–92, 1985.

[34] T. Sato and K. Ogawa, "New accelerating method for photon transport in Monte Carlo simulation," in *Proc. IEEE Nuclear Sci. Symp. Medical Imaging Conf.*, 1999, vol. 3, pp. 1851–1855.

[35] S. V. Patwardhan, S. Dai, and A. P. Dhawan, "Multi-spectral image analysis and classification of melanoma using fuzzy membership based partitions," *Computerized Medical Imaging Graphics*, vol. 29, no. 4, pp. 287–296, 2005.

[36] S. V. Patwardhan, "Multi-Spectral light interaction modeling and imaging of skin lesions," New Jersey Inst. Technol. Rep., 2004.

[37] R. A. Sheth *et al.*, "Real-time multichannel imaging framework for endoscopy, catheters,and fixed geometry intraoperative systems," *Molecular Imaging*, vol. 6, no. 3, pp. 147–155, 2007.

[38] J. Chang, H. L. Graber, and R. L. Barbour, "Imaging of fluorescence in highly scattering media," *IEEE Trans. Biomed. Eng.*, vol. 44, no. 5, pp. 810–822, May 1997.

[39] D. Y. Churmakov *et al.*, "Analysis of skin tissues spatial fluorescence distribution by the Monte Carlo simulation," *J. Phys. D: Appl. Phys.*, vol. 36, no. 14, pp. 1722–1728, 2003.

[40] S. V. Patwardhan, W. J. Akers, and D.-S. Bloch, "Fluorescence molecular Imaging: Microscopic to macroscopic," in *Prinicples and Advanced Methods in Medical Imaging and Image Analysis*, A. P. Dhawan, H. K. Huang, and D. Kim, Eds. Singapore, Singapore: World Scienitific, 2008, pp. 311–336.

[41] B. Selkin *et al.*, "*In vivo* confocal microscopy in dermatology," *Dermatologic Clinics*, vol. 19, no. 2, pp. 369–377, 2001.

[42] H. Inoue *et al.*, "A novel method of virtual histopathology using laser-scanning confocal microscopy in-vitro with untreated fresh specimens from the gastrointestinal mucosa," *Endoscopy*, vol. 32, no. 6, pp. 439–443, 2000.

[43] L. Oliveira-Soto and N. Efron, "Morphology of corneal nerves using confocal microscopy," *Cornea*, vol. 20, no. 4, pp. 374–384, 2001.

[44] G. Pellacani, A. M. Cesinaro, and S. Seidenari, "*In vivo* assessment of melanocytic nests in nevi and melanomas by reflectance confocal microscopy," *Modern Pathol.*, vol. 18, no. 4, pp. 469–474, 2005.

[45] A. L. Polglase *et al.*, "A fluorescence confocal endomicroscope for *in vivo* microscopy of the upper- and the lower-GI tract," *Gastrointestinal Endoscopy*, vol. 62, no. 5, pp. 686–695, 2005.

[46] M. Huzaira *et al.*, "Topographic variations in normal skin, as viewed by *in vivo* reflectance confocal microscopy," *J. Investigative Dermatol.*, vol. 116, no. 6, pp. 846–852, 2001.

[47] P. J. Caspers, G. W. Lucassen, and G. J. Puppels, "Combined *in vivo* confocal Raman spectroscopy and confocal microscopy of human skin," *Biophys. J.*, vol. 85, no. 1, pp. 572–580, 2003.

[48] D. S. Miller *et al.*, "Xenobiotic transport across isolated brain microvessels studied by confocal microscopy," *Molecular Pharmacol.*, vol. 58, no. 6, pp. 1357–1367, 2000.

[49] M. Brissova *et al.*, "Assessment of human pancreatic islet architecture and composition by laser scanning confocal microscopy," *J. Histochemistry Cytochemistry*, vol. 53, no. 9, pp. 1087–1097, 2005.

[50] T. Collier *et al.*, "Sources of scattering in cervical tissue: Determination of the scattering coefficient by confocal microscopy," *Appl. Opt.*, vol. 44, no. 11, pp. 2072–2081, 2005.

[51] H. Ra *et al.*, "Two-dimensional MEMS scanner for dual-axes confocal microscopy," *J. Microelectromechanical Syst.*, vol. 16, pp. 969–976, 2007.

[52] R. A. Drezek *et al.*, "Laser scanning confocal microscopy of cervical tissue before and after application of acetic acid," *Amer. J. Obstetrics Gynecol.*, vol. 182, no. 5, pp. 1135–1139, 2000.

[53] M. Sakashita *et al.*, "Virtual histology of colorectal lesions using laser-scanning confocal microscopy," *Endoscopy*, vol. 35, no. 12, pp. 1033–1038, 2003.

[54] P. S. P. Thong *et al.*, "Laser confocal endomicroscopy as a novel technique for fluorescence diagnostic imaging of the oral cavity," *J. Biomed. Opt.*, vol. 12, no. 1, 2007.

[55] G. Pellacani, A. M. Cesinaro, and S. Seidenari, "Reflectance-mode confocal microscopy of pigmented skin lesions-improvement in melanoma diagnostic specificity," *J. Amer. Acad. Dermatol.*, vol. 53, no. 6, pp. 979–985, 2005.

[56] T. J. Farrell and M. S. Patterson, "Diffusion modeling of fluroescence in tissue," in *Handbook of Biomedical Fluorescence*, M. Mycek and B. Pogue, Eds. New York: Marcel-Dekker, 2003, pp. 29–60.

[57] E. Endlicher and H. Messmann, "Spectroscopy and fluorescence imaging," *Techniques Gastrointestinal Endoscopy*, vol. 5, no. 2, pp. 74–77, 2003.

[58] W. Denk, J. H. Strickler, and W. W. Webb, "Two-photon laser scanning fluorescence microscopy," *Science*, vol. 248, no. 4951, pp. 73–76, 1990.

[59] K. Konig, "Multiphoton microscopy in life sciences," *J. Microscopy*, vol. 200, no. 2, pp. 83–104, 2000.

[60] R. M. Williams, W. R. Zipfel, and W. W. Webb, "Multiphoton microscopy in biological research," *Current Opinion Chemical Biol.*, vol. 5, no. 5, pp. 603–608, 2001.

[61] F. Helmchen and W. Denk, "New developments in multiphoton microscopy," *Current Opinion Neurobiol.*, vol. 12, no. 5, pp. 593–601, 2002.

[62] W. R. Zipfel, R. M. Williams, and W. W. Webb, "Nonlinear magic: Multiphoton microscopy in the biosciences," *Nature Biotechnol.*, vol. 21, no. 11, pp. 1369–1377, 2003.

[63] M. Rubart, "Two-photon microscopy of cells and tissue," *Circulation Res.*, vol. 95, no. 12, pp. 1154–1166, 2004.

[64] F. Helmchen and W. Denk, "Deep tissue two-photon microscopy," *Nature Methods*, vol. 2, no. 12, pp. 932–940, 2005.

[65] J. C. Jung and M. J. Schnitzer, "Multiphoton endoscopy," *Opt. Lett.*, vol. 28, no. 11, pp. 902–904, 2003.

[66] M. Straub *et al.*, "Live cell imaging by multifocal multiphoton microscopy," *Eur. J. Cell Biol.*, vol. 79, no. 10, pp. 726–734, 2000.

[67] F. Stracke *et al.*, "Multiphoton microscopy for the investigation of dermal penetration of nanoparticle-borne drugs," *J. Investigative Dermatol.*, vol. 126, no. 10, pp. 2224–2233, 2006.

[68] M. D. Cahalan and I. Parker, "Choreography of cell motility and interaction dynamics imaged by two-photon microscopy in lymphoid organs," *Ann. Rev. Immunol.*, pp. 585–626, 2008.

[69] C. L. Phillips *et al.*, "Three-dimensional imaging of embryonic mouse kidney by two-photon microscopy," *Amer. J. Pathol.*, vol. 158, no. 1, pp. 49–55, 2001.

[70] G. D. Reddy *et al.*, "Three-dimensional random access multiphoton microscopy for functional imaging of neuronal activity," *Nature Neurosci.*, vol. 11, no. 6, pp. 713–720, 2008.

[71] B. R. Masters and P. T. C. So, "Confocal microscopy and multi-photon excitation microscopy of human skin *in vivo*," *Opt. Expr.*, vol. 8, no. 1, pp. 2–10, 2001.

[72] R. Kurtz *et al.*, "Application of multiline two-photon microscopy to functional *in vivo* imaging," *J. Neurosci. Methods*, vol. 151, no. 2, pp. 276–286, 2006.

[73] R. Salomac *et al.*, "Ultrafast random-access scanning in two-photon microscopy using acousto-optic deflectors," *J. Neurosci. Methods*, vol. 154, no. 1–2, pp. 161–174, 2006.

[74] K. W. Dunn *et al.*, "Functional studies of the kidney of living animals using multicolor two-photon microscopy," *Amer. J. Physiology—Cell Physiol.*, vol. 283, no. 3, pp. 52–53, 2002.

[75] M. J. Levene *et al.*, "*In vivo* multiphoton microscopy of deep brain tissue," *J. Neurophysiol.*, vol. 91, no. 4, pp. 1908–1912, 2004.

[76] D. Bird and M. Gu, "Compact two-photon fluorescence microscope based on a single-mode fiber coupler," *Opt. Lett.*, vol. 27, no. 12, pp. 1031–1033, 2002.

[77] D. Bird and M. Gu, "Two-photon fluorescence endoscopy with a micro-optic scanning head," *Opt. Lett.*, vol. 28, no. 17, pp. 1552–1554, 2003.

[78] H. Bao *et al.*, "Fast handheld two-photon fluorescence microendoscope with a 475 Î1/4 m Ã–475 Î1/4 m field of view for *in vivo* imaging," *Opt. Lett.*, vol. 33, no. 12, pp. 1333–1335, 2008.

[79] M. T. Myaing, D. J. MacDonald, and X. Li, "Fiber-optic scanning two-photon fluorescence endoscope," *Opt. Lett.*, vol. 31, no. 8, pp. 1076–1078, 2006.

[80] S. Tang *et al.*, "Multiphoton endoscope using MEMS scanner," in *Proc. 30th Ann. Int. Conf. IEEE Eng. Medicine Biology Society, EMBS'08.*, pp. 1853–1853.

[81] H. Bao and M. Gu, "Reduction of self-phase modulation in double-clad photonic crystal fiber for nonlinear optical endoscopy," *Opt. Lett.*, vol. 34, no. 2, pp. 148–150, 2009.

[82] M. C. Skala *et al.*, "Multiphoton microscopy of endogenous fluorescence differentiates normal, precancerous, and cancerous squamous epithelial tissues," *Cancer Res.*, vol. 65, no. 4, pp. 1180–1186, 2005.

[83] I. Pastirk *et al.*, "Selective two-photon microscopy with shaped femtosecond pulses," *Opt. Expr.*, vol. 11, no. 14, pp. 1695–1701, 2003.

[84] M. Oheim *et al.*, "Two-photon microscopy in brain tissue: Parameters influencing the imaging depth," *J. Neurosci. Methods*, vol. 111, no. 1, pp. 29–37, 2001.

[85] P. N. Marsh, D. Burns, and J. M. Girkin, "Practical implementation of adaptive optics in multiphoton microscopy," *Opt. Expr.*, vol. 11, no. 10, pp. 1123–1130, 2003.

[86] B. J. Reid *et al.*, "Optimizing endoscopic biopsy detection of early cancers in Barrett's high-grade dysplasia," *Amer. J. Gastroenterol.*, vol. 95, no. 11, pp. 3089–3096, 2000.

[87] J. J. G. H. M. Bergman and G. N. J. Tytgat, "New developments in the endoscopic surveillance of Barrett's oesophagus," *Gut*, vol. 54, no. Suppl. 1, 2005.

[88] V. Nadeau *et al.*, "A compact endoscopic fluorescence detection system for gastro-intestinal cancers," *Opt. Methods Tumor Treatment Detection: Mechanisms Techniques Photodynamic Therapy X.*, pp. 91–96.

[89] U. Sukowski *et al.*, "Endoscopic detection of early malignancies in the upper gastrointestinal tract using laser-induced fluorescence imaging," *Clinical Lasers Diagnostics.*, pp. 255–261.

[90] M. Csanády *et al.*, "ALA (5-aminolevulinic acid)-induced protoporphyrin IX fluorescence in the endoscopic diagnostic and control of pharyngo-laryngeal cancer," *Eur. Archives Oto-Rhino-Laryngol.*, vol. 261, no. 5, pp. 262–266, 2004.

[91] W. Zheng *et al.*, "Detection of squamous cell carcinomas and precancerous lesions in the oral cavity by quantification of 5-aminolevulinic acid induced fluorescence endoscopic images," *Lasers Surgery Medicine*, vol. 31, no. 3, pp. 151–157, 2002.

[92] R. J. McNichols *et al.*, "Development of an endoscopic fluorescence image guided OCT probe for oral cancer detection," *Biomed. Diagnostic, Guidance, Surgical-Assist Systems III*, pp. 23–30.

[93] J. Beuthan *et al.*, "Optical fluorescence and X-ray fluorescence endoscopic imaging—Comparison and basic investigations," *Medical Laser Applic.*, vol. 21, no. 1, pp. 67–74, 2006.

[94] A. Divetia *et al.*, "Dynamically focused optical coherence tomography for endoscopic applications," *Appl. Phys. Lett.*, vol. 86, no. 10, pp. 1–3, 2005.

[95] K. Aljasem *et al.*, "Fiber optic tunable probe for endoscopic optical coherence tomography," *J. Optics A: Pure Appl. Opt.*, vol. 10, no. 4, 2008.

[96] T. Xie *et al.*, "GRIN lens rod based probe for endoscopic spectral domain optical coherence tomography with fast dynamic focus tracking," *Opt. Expr.*, vol. 14, no. 8, pp. 3238–3246, 2006.

[97] Y. Pan, H. Xie, and G. K. Fedder, "Endoscopic optical coherence tomography based on a microelectromechanical mirror," *Opt. Lett.*, vol. 26, no. 24, pp. 1966–1968, 2001.

[98] W. Piyawattanametha *et al.*, "Two-dimensional endoscopic MEMS scanner for high resolution optical coherence tomography," in *Proc. Conf. Lasers Electro-Optics, CLEO*, pp. 1661–1663.

[99] H. Xie, G. K. Fedder, and Y. Pan, "MEMS based endoscopic optical coherence tomography," *MOEMS Display Imaging Systems III*, pp. 81–92.

[100] Z. Chen *et al.*, "High speed three-dimensional endoscopic OCT using MEMS technology," in *Proc. SPIE Int. Soc. Opt. Eng.—MOEMS Miniaturized Systems VI*, San Jose, CA, 2007.

[101] P. H. Tran *et al.*, "*In vivo* endoscopic optical coherence tomography by use of a rotational microelectromechanical system probe," *Opt. Lett.*, vol. 29, no. 11, pp. 1236–1238, 2004.

[102] E. J. Seibel *et al.*, "Scanning single fiber endoscopy: A new platform technology for integrated laser imaging, diagnosis,and future therapies," *Gastrointestinal Endoscopy Clinics North Amer.*, vol. 18, no. 3, pp. 467–478, 2008.

[103] E. J. Seibel *et al.*, "Tethered capsule endoscopy: A low-cost and high-performance alternative technology for the screening of esophageal cancer and Barrett's esophagus," *IEEE Trans. Biomed. Eng.*, vol. 55, no. 11, pp. 1032–1042, Nov. 2008.

[104] J. M. Zara and P. E. Patterson, "Polyimide amplified piezoelectric scanner for endoscopic optical coherence tomography," in *Proc. SPIE Int. Soc. Opt. Eng.*, San Jose, CA, 2006.

[105] Y. Xu *et al.*, "MEMS based non-rotatory circumferential scanning optical probe for endoscopic optical coherence tomography," in *Proc. SPIE Progr. Biomed. Opt. Imaging*, Munich, Germany, 2007.

[106] L. Wu and H. Xie, "A dual reflective electrothermal MEMS micromirror for full circumferential scanning endoscopic imaging," in *Proc. SPIE Int. Soc. Opt. Eng.*, San Jose, CA, 2008, .

[107] G. Cinalli *et al.*, "Current state and future development of intracranial neuroendoscopic surgery," *Expert Rev. Medical Devices*, vol. 2, no. 3, pp. 351–373, 2005.

[108] Y. Tamura *et al.*, "Endoscopic identification and biopsy sampling of an intraventricular malignant glioma using a 5-aminolevulinic acid-induced protoporphyrin IX fluorescence imaging system. Technical note," *J. Neurosurgery*, vol. 106, no. 3, pp. 507–510, 2007.

[109] V. X. D. Yang *et al.*, "High speed, wide velocity dynamic range doppler optical coherence tomography (part III): *In vivo* endoscopic imaging of blood flow in the rat and human gastrointestinal tracts," *Opt. Expr.*, vol. 11, no. 19, pp. 2416–2424, 2003.

[110] V. X. D. Yang *et al.*, "Endoscopic Doppler optical coherence tomography in the human GI tract: Initial experience," *Gastrointestinal Endoscopy*, vol. 61, no. 7, pp. 879–890, 2005.

[111] J. G. Fujimoto *et al.*, "Optical biopsy and imaging using optical coherence tomography," *Nature Medicine*, vol. 1, no. 9, pp. 970–972, 1995.

[112] D. Huang *et al.*, "Optical coherence tomography," *Science*, vol. 254, no. 5035, pp. 1178–1181, 1991.

[113] A. F. Low *et al.*, "Technology insight: Optical coherence tomography—Current status and future development," *Nature Clinical Practice Cardiovascular Medicine*, vol. 3, no. 3, pp. 154–162, 2006.

[114] K. Sokolov *et al.*, "Optical systems for *in vivo* molecular imaging of cancer," *Technol. Cancer Res. Treatment*, vol. 2, no. 6, pp. 491–504, 2003.

[115] J. M. Schmitt, "Optical coherence tomography (OCT): A review," *IEEE J. Sel. Topics Quantum Electron.*, vol. 5, no. 4, pp. 1205–1215, 1999.

[116] W. Drexler and J. Fujimoto, *Optical Coherence Tomography: Technological Applications*. New York: Springer, 2008.

[117] J. G. Fujimoto *et al.*, "Femtosecond optical ranging in biological systems," *Opt. Lett.*, vol. 11, no. 3, pp. 150–152, 1986.

[118] M. R. Hee *et al.*, "Optical coherence tomography of the human retina," *Archives Ophthalmology*, vol. 113, no. 3, pp. 325–332, 1995.

[119] M. E. Brezinski and J. G. Fujimoto, "Optical coherence tomography: High-resolution imaging in nontransparent tissue," *IEEE J. Sel. Topics Quantum Electron.*, vol. 5, no. 4, pp. 1185–1192, Apr. 1999.

[120] J. Bush, P. Davis, and M. A. Marcus, "All-fiber optic coherence domain interferometric techniques," *Fiber Optic Sensor Technol. II*, pp. 71–80.

[121] Z. Ding *et al.*, "High-resolution optical coherence tomography over a large depth range with an axicon lens," *Opt. Lett.*, vol. 27, no. 4, pp. 243–245, 2002.

[122] W. Drexler *et al.*, "*In vivo* ultrahigh-resolution optical coherence tomography," *Opt. Lett.*, vol. 24, no. 17, pp. 1221–1223, 1999.

[123] J. G. Fujimoto, "Optical coherence tomography for ultrahigh resolution *in vivo* imaging," *Nature Biotechnol.*, vol. 21, no. 11, pp. 1361–1367, 2003.

[124] J. A. Izatt *et al.*, "Micrometer-scale resolution imaging of the anterior eye *in vivo* with optical coherence tomography," *Archives Ophthalmol.*, vol. 112, no. 12, pp. 1584–1589, 1994.

[125] S. Jackle *et al.*, "*In vivo* endoscopic optical coherence tomography of the human gastrointestinal tract—Toward optical biopsy," *Endoscopy*, vol. 32, no. 10, pp. 743–749, 2000.

[126] S. J. Kim and N. M. Bressler, "Optical coherence tomography and cataract surgery," *Current Opinion Ophthalmol.*, vol. 20, no. 1, pp. 46–51, 2009.

[127] T. M. Lee *et al.*, "Engineered microsphere contrast agents for optical coherence tomography," *Opt. Lett.*, vol. 28, no. 17, pp. 1546–1548, 2003.

[128] G. J. Tearney *et al.*, "*In vivo* endoscopic optical biopsy with optical coherence tomography," *Science*, vol. 276, no. 5321, pp. 2037–2039, 1997.

[129] R. K. Wang and J. B. Elder, "Propylene glycol as a contrasting agent for optical coherence tomography to image gastrointestinal tissues," *Lasers Surgery Medicine*, vol. 30, no. 3, pp. 201–208, 2002.

[130] Y. Wang *et al.*, "Photoacoustic tomography of a nanoshell contrast agent in the *in vivo* rat brain," *Nano Lett.*, vol. 4, no. 9, pp. 1689–1692, 2004.

[131] B. E. Bouma and G. J. Tearney, *Handbook on Optical Coherence Tomography*. New York: Marcel Dekker, 2002.

[132] R. Beddows, S. W. James, and R. P. Tatam, "Improved performance interferometer designs for optical coherence tomography," in *Proc. 15th Int. Conf. Optical Fibre Sensors (OFS-15)*, 2002, pp. 527–530.

[133] P. Casaubieilh, H. D. Ford, and R. P. Tatam, "Optical fibre fizeau-based OCT," in *Proc. Second Eur. Workshop Optical Fibre Sensors, EWOFS'04.*, pp. 338–341.

[134] J. U. Kang *et al.*, "Endoscopic functional Fourier domain common-path optical coherence tomography for microsurgery," *IEEE J. Sel. Topics Quantum Electron.*, 2010, to be published.

[135] X. Li *et al.*, "Signal-to-noise ratio analysis of all-fiber common-path optical coherence tomography," *Appl. Opt.*, vol. 47, no. 27, pp. 4833–4840, 2008.

[136] X. Liu *et al.*, "Fiber-optic Fourier-domain common-path OCT," *Chinese Opt. Lett.*, vol. 6, no. 12, pp. 899–901, 2008.

[137] U. Sharma and J. U. Kang, "Common-path optical coherence tomography with side-viewing bare fiber probe for endoscopic optical coherence tomography," *Rev. Scientific Instruments*, vol. 78, no. 11, 2007.

[138] K. M. Tan *et al.*, "In-fiber common-path optical coherence tomography using a conical-tip fiber," *Opt. Expr.*, vol. 17, no. 4, pp. 2375–2384, 2009.

[139] A. R. Tumlinson *et al.*, "Endoscope-tip interferometer for ultrahigh resolution frequency domain optical coherence tomography in mouse colon," *Opt. Expr.*, vol. 14, no. 5, pp. 1878–1887, 2006.

[140] A. B. Vakhtin *et al.*, "Common-path interferometer for frequency-domain optical coherence tomography," *Appl. Opt.*, vol. 42, no. 34, pp. 6953–6958, 2003.

[141] S. Vergnole *et al.*, "Common path swept-source OCT interferometer with artifact removal," in *Proc. SPIE*, San Jose, CA, 2008, 68472W.

[142] J.-H. Han *et al.*, "Common-path Fourier-domain optical coherence tomography with a fiber optic probe integrated into a surgical needle," in *OSA Tech. Dig. Conf. Lasers Electro-Optics/Int. Quantum Electronics*, Baltimore, MD, 2009.

[143] K. Zhang *et al.*, "A surface topology and motion compensation system for microsurgery guidance and intervention based on common-path optical coherence tomography," *IEEE Trans. Biomed. Eng.*, vol. 56, no. 11, pp. 2318–2321, Nov. 2009.

[144] J. A. Izatt *et al.*, "Optical coherence tomography and microscopy in gastrointestinal tissues," *IEEE J. Sel. Topics Quantum Electron.*, vol. 2, no. 4, pp. 1017–1028, Apr. 1996.

[145] G. J. Tearney *et al.*, "Scanning single-mode fiber optic catheter-endoscope for optical coherence tomography," *Opt. Lett.*, vol. 21, no. 7, pp. 543–545, 1996.

[146] M. V. Sivak, Jr *et al.*, "High-resolution endoscopic imaging of the GI tract using optical coherence tomography," *Gastrointestinal Endoscopy*, vol. 51, no. 4 I, pp. 474–479, 2000.

[147] V. Westphal *et al.*, "Correlation of endoscopic optical coherence tomography with histology in the lower-GI tract," *Gastrointestinal Endoscopy*, vol. 61, no. 4, pp. 537–546, 2005.

[148] A. Das *et al.*, "High-resolution endoscopic imaging of the GI tract: A comparative study of optical coherence tomography versus high-frequency catheter probe EUS," *Gastrointestinal Endoscopy*, vol. 54, no. 2, pp. 219–224, 2001.

[149] J. M. Zara and C. A. Lingley-Papadopoulos, "Endoscopic OCT approaches toward cancer diagnosis," *IEEE J. Sel. Topics Quantum Electron.*, vol. 14, no. 1, pp. 70–81, Jan. 2008.

[150] X. D. Li *et al.*, "Optical coherence tomography: Advanced technology for the endoscopic imaging of Barrett's esophagus," *Endoscopy*, vol. 32, no. 12, pp. 921–930, 2000.

[151] Y. Chen *et al.*, "Ultrahigh resolution optical coherence tomography of Barrett's esophagus: Preliminary descriptive clinical study correlating images with histology," *Endoscopy*, vol. 39, no. 7, pp. 599–605, 2007.

[152] G. Isenberg *et al.*, "Accuracy of endoscopic optical coherence tomography in the detection of dysplasia in Barrett's esophagus: A prospective, double-blinded study," *Gastrointestinal Endoscopy*, vol. 62, no. 6, pp. 825–831, 2005.

[153] X. Qi *et al.*, "Computer-aided diagnosis of dysplasia in Barrett's esophagus using endoscopic optical coherence tomography," *J. Biomed. Opt.*, vol. 11, no. 4, 2006.

[154] E. Zagaynova *et al.*, "Endoscopic OCT with forward-looking probe: Clinical studies in urology and gastroenterology," *J. Biophoton.*, vol. 1, no. 2, pp. 114–128, 2008.

[155] A. P. Dhawan, N. Mullani, and S. Patwardhan, "Analysis of multi-modal optical images of skin-lesions for skin-cancer detection and characterization," in *Proc. 5th Int. Conf. Information Technology and Applications in Biomedicine, ITAB 2008 in Conjunction with 2nd Int. Symp. Summer School Biomed. Health Eng., IS3BHE*, 2008, pp. 62–65.

[156] V. Terushkin *et al.*, "Transillumination as a means to differentiate melanocytic lesions based upon their vascularity," *Archives Dermatol.*, vol. 145, no. 9, pp. 1060–1062, 2009.

[157] S. Wang and A. P. Dhawan, "Shape-based multi-spectral optical image reconstruction through genetic algorithm based optimization," *Computerized Medical Imaging Graphics*, vol. 32, no. 6, pp. 429–441, 2008.

[158] C. Yang, "Developing new biomedical imaging modalities through the applications of novel optical concepts," in *Proc. 2004 IEEE LEOS Annu. Meeting*, Rio Grande, Puerto Rico, 2004, pp. 863–864.

[159] T. J. Pfefer *et al.*, "Reflectance-based determination of optical properties in highly attenuating tissue," *J. Biomed. Opt.*, vol. 8, no. 2, pp. 206–215, 2003.

[160] J. M. Yang, F. Laager, and K. S. Soh, "Investigation of diffuse reflectance of tissues *in vivo* with backscattering fiber probe and multi-channel diffuse reflectance imaging system," in *Proc. 2007 Conf. Lasers Electro-Optics—Pacific Rim, CLEO/PACIFIC RIM*.

[161] S. V. Patwardhan, A. P. Dhawan, and P. A. Relue, "Monte Carlo simulation of light-tissue interaction: Three-dimensional simulation for trans-illumination-based imaging of skin lesions," *IEEE Trans. Biomed. Eng.*, vol. 52, no. 5, pp. 1227–1236, May 2005.

[162] V. Ntziachristos, C. Bremer, and R. Weissleder, "Fluorescence imaging with near-infrared light: New technological advances that enable *in vivo* molecular imaging," *Eur. Radiol.*, vol. 13, no. 1, pp. 195–208, 2003.

[163] V. Ntziachristos and J. Ripoll, "Optical molecular imaging," in *Proc. Saratov Fall Meeting 2003—Optical Technologies Biophysics Medicine V.*, pp. 224–234.

[164] M. C. Pan, C. H. Chen, and L. Y. Chen, "Filtering effect to improve the reconstructed image quality of diffuse optical imaging," in *Proc. SPIE Progr. Biomed. Opt. Imaging*, Munich, Germany, 2007.

[165] B. W. Pogue *et al.*, "Initial assessment of a simple system for frequency domain diffuse optical tomography," *Phys. Medicine Biol.*, vol. 40, no. 10, pp. 1709–1729, 1995.

[166] V. Ntziachristos and R. Weissleder, "Experimental three-dimensional fluorescence reconstruction of diffuse media by use of a normalized born approximation," *Opt. Lett.*, vol. 26, no. 12, pp. 893–895, 2001.

[167] C. P. Gonatas *et al.*, "Optical diffusion imaging using a direct inversion method," *Phys. Rev. E*, vol. 52, no. 4, pp. 4361–4365, 1995.

[168] A. P. Gibson, J. C. Hebden, and S. R. Arridge, "Recent advances in diffuse optical imaging," *Phys. Medicine Biol.*, vol. 50, no. 4, 2005.

[169] S. R. Arridge, "Optical tomography in medical imaging," *Inverse Problems*, vol. 15, no. 2, 1999.

[170] M. A. O'Leary *et al.*, "Experimental images of heterogeneous turbid media by frequency-domain diffusing-photon tomography," *Opt. Lett.*, vol. 20, no. 5, pp. 426–428, 1995.

[171] Y. Yao *et al.*, "Frequency-domain optical imaging of absorption and scattering distributions by a born iterative method," *J. Opt. Soc. Amer. A: Optics Image Science Vision*, vol. 14, no. 1, pp. 325–342, 1997.

[172] R. J. Gaudette *et al.*, "A comparison study of linear reconstruction techniques for diffuse optical tomographic imaging of absorption coefficient," *Phys. Medicine Biol.*, vol. 45, no. 4, pp. 1051–1070, 2000.

[173] B. W. Pogue *et al.*, "Spatially variant regularization improves diffuse optical tomography," *Appl. Opt.*, vol. 38, no. 13, pp. 2950–2961, 1999.

[174] J. C. Ye *et al.*, "Modified distorted born iterative method with an approximate fréchet derivative for optical diffusion tomography," *J. Opt. Soc. Amer. A: Optics Image Sci., Vision*, vol. 16, no. 7, pp. 1814–1826, 1999.

[175] A. H. Hielscher, A. D. Klose, and K. M. Hanson, "Gradient-based iterative image reconstruction scheme for time-resolved optical tomography," *IEEE Trans. Medical Imaging*, vol. 18, no. 2, pp. 262–271, Feb. 1999.

[176] A. Y. Bluestone *et al.*, "Three-dimensional optical tomography of hemodynamics in the human head," *Opt. Expr.*, vol. 9, no. 6, pp. 272–286, 2001.

[177] R. Roy and E. M. Sevick-Muraca, "A numerical study of gradient-based nonlinear optimization methods for contrast enhanced optical tomography," *Opt. Expr.*, vol. 9, no. 1, pp. 49–65, 2001.

[178] A. Soubret, J. Ripoll, and V. Ntziachristos, "Accuracy of fluorescent tomography in the presence of heterogeneities: Study of thenormalized born ratio," *IEEE Trans. Medical Imaging*, vol. 24, no. 9, pp. 1377–1386, Sep. 2005.

[179] M. Gurfinkel *et al.*, "Pharmacokinetics of ICG and HPPH-car for the detection of normal and tumor tissue using fluorescence, near-infrared reflectance imaging: A case study," *Photochemistry Photobiol.*, vol. 72, no. 1, pp. 94–102, 2000.

[180] K. Licha *et al.*, "Hydrophilic cyanine dyes as contrast agents for near-infrared tumor imaging: Synthesis photophysical properties and spectroscopic *In vivo* characterization," *Photochemistry Photobiol.*, vol. 72, no. 3, pp. 392–398, 2000.

[181] A. Godavarty *et al.*, "Diagnostic imaging of breast cancer using fluorescence-enhanced optical tomography: Phantom studies," *J. Biomed. Opt.*, vol. 9, no. 3, pp. 488–496, 2004.

[182] E. V. Zagaynova *et al.*, "Optical coherence tomography in guided surgery of GI cancer," *Photonic Therapeutics Diagnostics*, pp. 367–374.

[183] E. V. Zagaynova *et al.*, "*In vivo* optical coherence tomography feasibility for bladder disease," *J. Urol.*, vol. 167, no. 3, pp. 1492–1496, 2002.

[184] E. V. Zagaynova *et al.*, "Combined use of optical coherence tomography and fluorescence cystoscopy to detect bladder neoplasia," in *Proc. SPIE Progr. Biomed. Opt. Imaging*, San Jose, CA, 2006.

[185] A. Corlu *et al.*, "Three-dimensional *in vivo* fluorescence diffuse optical tomography of breast cancer in humans," *Opt. Expr.*, vol. 15, no. 11, pp. 6696–6716, 2007.

[186] M. D. M. Cutler, "Transillumination of breasts," *J. Amer. Med. Assoc.*, vol. 93, no. 21, p. 1671, 1929.

[187] J. E. Martin, "Breast imaging techniques. Mammography ultrasonography, computed tomography, thermography, and transillumination," *Radiol. Clin. North Amer.*, vol. 21, no. 1, pp. 53–149, 1983.

[188] D. J. Watmough, "Transillumination of breast tissues: Factors governing optimal imaging of lesions," *Radiology*, vol. 147, no. 1, pp. 89–92, Apr. 1983.

[189] G. Jarry *et al.*, "Imaging mammalian tissues and organs using laser collimated transillumination," *J Biomed Eng*, vol. 6, no. 1, pp. 4–70, 1984.

[190] H. Key, P. C. Jackson, and P. N. Wells, "New approaches to transillumination imaging," *J. Biomed. Eng.*, vol. 10, no. 2, pp. 8–113, Apr. 1988.

[191] R. J. Grable *et al.*, "Optical computed tomography for imaging the breast: First look," *Optical Sensing, Imaging, Manipulation for Biological Biomedical Applic.*, pp. 40–45.

[192] L. Wang *et al.*, "Optimizing single projection linear tomographic optical breast imaging," *Optical Tomography Spectroscopy Tissue IV*, pp. 391–406.

[193] B. J. Tromberg *et al.*, "Diffuse optics in breast cancer: Detecting tumors in pre-menopausal women and monitoring neoadjuvant chemotherapy," *Breast Cancer Res.*, vol. 7, no. 6, pp. 279–285, 2005.

[194] D. A. Young and J. D. Featherstone, "Digital imaging fiber-optic trans-illumination, F-speed radiographic film and depth of approximal lesions," *J. Amer. Dental Assoc.*, vol. 136, no. 12, pp. 7–1682, 2005.

[195] Q. Zhang *et al.*, "Coregistered tomographic X-ray and optical breast imaging: Initial results," *J. Biomed. Opt.*, vol. 10, no. 2, pp. 1–9, 2005.

[196] S. G. Demos, A. J. Vogel, and A. H. Gandjbakhche, "Advances in optical spectroscopy and imaging of breast lesions," *J. Mammary Gland Biol. Neoplasia*, vol. 11, no. 2, pp. 165–181, 2006.

[197] D. R. Leff *et al.*, "Diffuse optical imaging of the healthy and diseased breast: A systematic review," *Breast Cancer Res. Treatment*, vol. 108, no. 1, pp. 9–22, 2008.

[198] L. S. Fournier *et al.*, "Dynamic optical breast imaging: A novel technique to detect and characterize tumor vessels," *Eur. J. Radiol.*, vol. 69, no. 1, pp. 43–49, 2009.
[199] L. D. Lilge, "Optical transillumination spectroscopy of breast tissue to determine cancer risk in pre and post-menopausal women," , submitted for publication.
[200] K. J. Blackmore KM, R. Jong, and L. Lilge, "Assessing breast tissue density by transillumination breast spectroscopy (TIBS): An intermediate indicator of cancer risk," *Brit. J. Radiol.*, vol. 80, no. 955, pp. 545–556, 2007.
[201] B. Chakravarti *et al.*, "A highly uniform UV transillumination imaging system for quantitative analysis of nucleic acids and proteins," *Proteomics*, vol. 8, no. 9, pp. 97–1789, May 2008.
[202] S. Gayen and R. Alfano, "Sensing lesions in tissues with light," *Opt. Expr.*, vol. 4, no. 11, pp. 475–480, May 1999.
[203] C. En, "Transillumination light scanning," *Diag. Imag.*, vol. 3, pp. 28–33, 1982.
[204] S. K. Gayen *et al.*, "Two-dimensional near-infrared transillumination imaging of biomedical media with a chromium-doped forsterite laser," *Appl. Opt.*, vol. 37, no. 22, pp. 5327–5336, 1998.
[205] O. Jarlman *et al.*, "Time-resolved white light transillumination for optical imaging," *Acta Radiol.*, vol. 38, no. 1, pp. 185–189, Jan. 1997.
[206] S. Behin-Ain, T. van Doorn, and J. R. Patterson, "First photon detection in time-resolved transillumination imaging: A theoretical evaluation," *Phys. Med. Biol.*, vol. 49, no. 17, pp. 3939–3955, Sep. 2004.
[207] A. H. Gandjbakhche *et al.*, "Time-dependent contrast functions for quantitative imaging in time-resolved transillumination experiments," *Appl. Opt.*, vol. 37, no. 10, pp. 1973–1981, Apr. 1998.
[208] K. Takagi, Y. Kato, and K. Shimizu, "Extraction of near-axis scattered light for transillumination imaging," *Appl. Opt.*, vol. 48, no. 10, pp. D36–D44, Apr. 2009.
[209] J. C. Hebden and R. A. Kruger, "Transillumination imaging performance: Spatial resolution simulation studies," *Med. Phys.*, vol. 17, no. 1, pp. 41–47, Jan.–Feb. 1990.
[210] J. C. Hebden and A. H. Gandjbakhche, "Experimental validation of an elementary formula for estimating spatial resolution for optical transillumination imaging," *Med. Phys.*, vol. 22, no. 8, pp. 1271–1272, Aug. 1995.
[211] T. Yuasa *et al.*, "Fundamental imaging properties of transillumination laser computed tomography based on coherent detection imaging method," *Anal. Sci.*, vol. 18, no. 12, pp. 1329–1333, Dec. 2002.
[212] J. A. Moon *et al.*, "Achievable spatial resolution of time-resolved transillumination imaging systems which utilize multiply scattered light," *Phys. Rev. E Stat. Phys. Plasmas Fluids Relat. Interdiscip. Topics*, vol. 53, no. 1, pp. 1142–1155, Jan. 1996.
[213] S. Behin-Ain, T. van Doorn, and J. R. Patterson, "Spatial resolution in fast time-resolved transillumination imaging: An indeterministic Monte Carlo approach," *Phys. Med. Biol.*, vol. 47, no. 16, pp. 2935–2945, Aug. 2002.
[214] A. Schneiderman *et al.*, "Assessment of dental caries with digital imaging fiber-optic transillumination (DIFOTI): *In vitro* study," *Caries Res.*, vol. 31, no. 2, pp. 103–110, 1997.
[215] S. Keem and M. Elbaum, "Wavelet representations for monitoring changes in teeth imaged with digital imaging fiber-optic transillumination," *IEEE Trans. Med. Imaging*, vol. 16, no. 5, pp. 653–663, Oct. 1997.
[216] R. Jones *et al.*, "Near-infrared transillumination at 1310-nm for the imaging of early dental decay," *Opt. Expr.*, vol. 11, no. 18, pp. 2259–2265, Sep. 2003.
[217] R. Srinivasan and M. Singh, "Laser backscattering and transillumination imaging of human tissues and their equivalent phantoms," *IEEE Trans. Biomed. Eng.*, vol. 50, no. 6, pp. 724–730, Jun. 2003.
[218] O. Bernus *et al.*, "Simulation of voltage-sensitive optical signals in three-dimensional slabs of cardiac tissue: Application to transillumination and coaxial imaging methods," *Phys. Med. Biol.*, vol. 50, no. 2, pp. 215–229, Jan. 2005.
[219] O. Bernus, K. S. Mukund, and A. M. Pertsov, "Detection of intramyocardial scroll waves using absorptive transillumination imaging," *J. Biomed. Opt.*, vol. 12, no. 1, pp. 014035–014035, Jan.–Feb. 2007.
[220] S. S. Dixit *et al.*, "Development of a transillumination infrared modality for differential vasoactive optical imaging," *Appl. Opt.*, vol. 48, no. 10, 2009.
[221] X. Liang *et al.*, "Phase-Contrast diffuse optical tomography. Pilot results in the breast," *Academic Radiol.*, vol. 15, no. 7, pp. 859–866, 2008.
[222] Y. Tan and H. Jiang, "DOT guided fluorescence molecular tomography of arbitrarily shaped objects," *Med. Phys.*, vol. 35, no. 12, pp. 5703–5707, 2008.
[223] Y. Tan and H. Jiang, "Diffuse optical tomography guided quantitative fluorescence molecular tomography," *Appl. Opt.*, vol. 47, no. 12, pp. 2011–2016, 2008.
[224] Q. Wang *et al.*, "Visualizing localized dynamic changes during epileptic seizure onset *in vivo* with diffuse optical tomography," *Med. Phys.*, vol. 35, no. 1, pp. 216–224, 2008.
[225] Q. Wang, Z. Liu, and H. Jiang, "Optimization and evaluation of a three-dimensional diffuse optical tomography system for brain imaging," *J. X-Ray Sci. Technol.*, vol. 15, no. 4, pp. 223–234, 2007.
[226] Z. Yuan, X. H. Hu, and H. Jiang, "A higher order diffusion model for three-dimensional photon migration and image reconstruction in optical tomography," *Phys. Med. Biol.*, vol. 54, no. 1, pp. 65–88, 2009.
[227] Q. Zhang *et al.*, "Three-Dimensional bioluminescence tomography assisted by diffuse optical tomography," in *OSA Tech. Dig. (CD)*, p. BSuE84.
[228] R. O. Esenaliev, A. A. Karabutov, and A. A. Oraevsky, "Sensitivity of laser opto-acoustic imaging in detection of small deeply embedded tumors," *IEEE J. Sel. Topics Quantum Electron.* , vol. 5, no. 4, pp. 981–988, 1999.
[229] C. G. A. Hoelen and F. F. M. De Mul, "Image reconstruction for photoacoustic scanning of tissue structures," *Appl. Opt.*, vol. 39, no. 31, pp. 5872–5883, 2000.
[230] C. G. A. Hoelen *et al.*, "Three-dimensional photoacoustic imaging of blood vessels in tissue," *Opt. Lett.*, vol. 23, no. 8, pp. 648–650, 1998.
[231] R. A. Kruger *et al.*, "Photoacoustic ultrasound (PAUS)—Reconstruction tomography," *Med. Phys.*, vol. 22, no. 10, pp. 1605–1609, 1995.
[232] A. A. Oraevsky *et al.*, "Laser opto-acoustic imaging of the breast: Detection of cancer angiogenesis," *Proc. 1999 Optical Tomography Spectroscopy Tissue III.*, pp. 352–363.
[233] Y. V. Zhulina, "Optimal statistical approach to optoacoustic image reconstruction," *Appl. Opt.*, vol. 39, no. 32, pp. 5971–5977, 2000.
[234] J. J. Niederhauser, *Real-Time Biomedical Optoacoustic Imaging*. Zurich, Switzerland: Swiss Federal Inst. Technology Zürich, 2004.
[235] L. V. Wang, "Tutorial on photoacoustic microscopy and computed tomography," *IEEE J. Sel. Topics Quantum Electron.*, vol. 14, no. 1, pp. 171–179, Jan. 2008.
[236] H. F. Zhang *et al.*, "Functional photoacoustic microscopy for high-resolution and noninvasive *in vivo* imaging," *Nature Biotechnol.*, vol. 24, no. 7, pp. 848–851, 2006.
[237] G. Ku *et al.*, "Thermoacoustic and photoacoustic tomography of thick biological tissues toward breast imaging," *Technol. Cancer Res. Treatment*, vol. 4, no. 5, pp. 559–565, 2005.
[238] G. Ku and L. V. Wang, "Deeply penetrating photoacoustic tomography in biological tissues enhanced with an optical contrast agent," *Opt. Lett.*, vol. 30, no. 5, pp. 507–509, 2005.
[239] X. Wang *et al.*, "Non-invasive laser-induced photoacoustic tomography for structural and functional imaging of the brain *in vivo*," *Nature Biotech.*, vol. 21, no. 7, 2003.
[240] M. L. Li *et al.*, "Simultaneous molecular and hypoxia imaging of brain tumors *in vivo* using spectroscopic photoacoustic tomography," *Proc. IEEE*, vol. 96, no. 3, pp. 481–489, Mar. 2008.
[241] Z. Yuan and H. Jiang, "Image reconstruction scheme that combines modified Newton method and efficient initial guess estimation for optical tomography of finger joints," *Appl. Opt.*, vol. 46, no. 14, pp. 2757–2768, 2007.
[242] Z. Yuan, H. Jiang, and P. Sciences, "Quantitative photoacoustic tomography," *Philosophical Trans. Roy. Soc. A: Mathematical*, vol. 367, no. 1900, pp. 3043–3054, 2009.
[243] Z. Yuan, Q. Wang, and H. Jiang, "Reconstruction of optical absorption coefficient maps of heterogeneous media by photoacoustic tomography coupled with diffusion equation based regularized Newton method," *Opt. Expr.*, vol. 15, no. 26, pp. 18076–18081, 2007.
[244] L. Yao, Y. Sun, and H. Jiang, "Quantitative photoacoustic tomography based on the radiative transfer equation," *Opt. Lett.*, vol. 34, no. 12, pp. 1765–1767, 2009.
[245] Z. Yuan and H. Jiang, "Simultaneous recovery of tissue physiological and acoustic properties and the criteria for wavelength selection in multispectral photoacoustic tomography," *Opt. Lett.*, vol. 34, no. 11, pp. 1714–1716, 2009.
[246] L. Yao and H. Jiang, "Finite-element-based photoacoustic tomography in time domain," *J. Optics A: Pure Appl. Opt.*, no. 8, pp. 085301–085301, 2009.
[247] Q. Zhang *et al.*, "Noninvasive imaging of epileptic seizures *in vivo* using photoacoustic tomography," *Phys. Med. Biol.*, 2008.
[248] C. Balas, "Review of biomedical optical imaging-a powerful, non-invasive, non-ionizing technology for improving *in vivo* diagnosis," *Measurement Sci. Technol.*, vol. 20, no. 10, pp. 104020–104020, 2009.

[249] S. J. Erickson and A. Godavarty, "Hand-held based near-infrared optical imaging devices: A review," *Med. Eng. Phys.*, vol. 31, no. 5, pp. 495–509, 2009.
[250] A. Gibson and H. Dehghani, "Diffuse optical imaging," *Philosophical Trans. Roy. Soc. A: Mathematical, Phys. Eng. Sci.*, vol. 367, no. 1900, pp. 3055–3072, 2009.
[251] J. Fujimoto and D. Farkas, *Biomedical Optical Imaging*. Oxford, U.K.: Oxford Univ. Press, 2009.
[252] D. Brady, *Opt. Imaging Spectroscopy*. New York: Wiley-Interscience, 2009.
[253] L. Wang, *Photoacoustic Imaging Spectroscopy*. Boca Raton, FL: CRC, 2009.
[254] S. C. Kaufman *et al.*, "Confocal microscopy: A report by the American Academy of Ophthalmology," *Ophthalmology*, vol. 111, no. 2, pp. 396–406, 2004.
[255] S. Yoshida *et al.*, "Optical biopsy of GI lesions by reflectance-type laser-scanning confocal microscopy," *Gastrointestinal Endoscopy*, vol. 66, no. 1, pp. 144–149, 2007.
[256] W. Jung *et al.*, "*In vivo* three-dimensional spectral domain endoscopic optical coherence tomography using a microelectromechanical system mirror," *Opt. Lett.*, vol. 32, no. 22, pp. 3239–3241, 2007.
[257] T. D. Wang and J. Van Dam, "Optical biopsy: A new frontier in endoscopic detection and diagnosis," *Clin. Gastroenterol. Hepatol.*, vol. 2, no. 9, pp. 744–753, 2004.
[258] Y. T. Pan *et al.*, "Enhancing early bladder cancer detection with fluorescence-guided endoscopic optical coherence tomography," *Opt. Lett.*, vol. 28, no. 24, pp. 2485–2487, 2003.
[259] V. Nadeau *et al.*, "Endoscopic fluorescence imaging and point spectroscopy system for the detection of gastro-intestinal cancers," *J. Modern Opt.*, vol. 49, no. 5–6, pp. 731–741, Sep. 2002.
[260] K. Gono, "Novel multifunctional endoscopic imaging system for support of early cancer diagnosis," in *Proc. 20th Annu. Meeting IEEE Lasers Electro-Optics Soc.*, pp. 69–70.
[261] L. V. Wang, "Prospects of photoacoustic tomography," *Med. Phys.*, vol. 35, no. 12, pp. 5758–5767, 2008.
[262] Y. Wang *et al.*, "Endoscopic spectral-domain polarization-sensitive optical coherence tomography system," in *Proc. Int. Symp. Photoelectronic Detection Imaging, ISPDI 2007: Photoelectronic Imaging Detection*.
[263] Z. G. Wang *et al.*, "Optical coherence tomography for noninvasive diagnosis of epithelial cancers," in *Proc. 28th Annu. Int. Conf. IEEE Eng. Medicine Biology Soc., EMBS'06.*, pp. 129–132.

Atam P. Dhawan (F'08) received the B.S. and M.S. degrees from the Indian Institute of Technology, Roorkee, and the Ph.D. degree from the University of Manitoba, all in electrical engineering.

From 1985 to 2000, he held faculty positions in Electrical and Computer Engineering and Radiology departments at the University of Houston, University of Cincinnati, University of Texas, University of Texas Medical Center (Dallas), and University of Toledo. In July 2000, he joined the New Jersey Institute of Technology, Newark, where he now serves as a Distinguished Professor of electrical and computer engineering and Associate Dean of Albert Dorman Honors College. He has published 200 research articles in refereed journals, books, and conference proceedings. His current research interests are medical imaging, multi-modality medical image analysis, adaptive learning and pattern recognition.

Dr. Dhawan is a recipient of the Martin Epstein Award (1984), National Institutes of Health FIRST Award (1988), Sigma-Xi Young Investigator Award (1992), University of Cincinnati Faculty Achievement Award (1994), and the prestigious IEEE Engineering in Medicine and Biology Early Career Achievement Award (1995) and University of Toledo Doermann Distinguished Lecture Award (1999). He is Senior Editor of IEEE TRANSACTIONS ON BIOMEDICAL ENGINEERING and Editor-In-Charge of IEEE TRANSACTIONS ON BIOMEDICAL ENGINEERING LETTERS. He has served on many IEEE EMBS professional committees and has delivered Workshops on Intelligent Biomedical Image Analysis in IEEE EMBS International Conferences (1996, 1997, 2000, 2003). He served as the Chair of the "Emerging Technologies Committee" of the IEEE-EMB Society from 1997 to 1999, and 2009 through 2010. He was the Chair of the "New Frontiers in Biomedical Engineering" Symposium at the World Congress 2000 on Medical Physics and Biomedical Engineering. He was the Conference Chair of the IEEE 28th International Conference of Engineering in Medicine and Biology Society held in New York from August 30 to September 3, 2006. He has served as American Liaison and EMBS Representative in the Steering Committee of International Symposium of Biomedical Imaging (2009 to present). He has chaired numerous NIH review panels. Currently, he chairs the NIH Chartered Study Section on Biomedical Computing and Health Informatics. He is a member of Sigma Xi and Eta Kappa Nu honor societies. He is listed in *Who's Who in the World, Who's Who in America, Who's Who in Engineering*, and *Who's Who Among America's Teachers*.

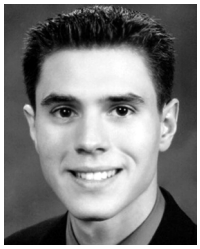

Brian D'Alessandro received the B.S. *(summa cum laude)* and M.S. degrees in computer engineering from the New Jersey Institute of Technology (NJIT), Newark, in 2008 and 2009, respectively. He is currently working toward the Ph.D. degree with the Department of Electrical and Computer Engineering at NJIT.

Since 2009, he has been a Teaching Assistant at NJIT. He has previous intern and research experience with IBM and the University of Medicine and Dentistry of New Jersey. His research interests include image processing, medical imaging, computer vision, digital signal processing, pattern classification, and audio quality detection.

Mr. D'Alessandro was selected as a Student Paper Competition Finalist in the International Conference of the IEEE Engineering in Medicine and Biology Society in 2010 for his work on oxygen saturation measurement of skin lesions. He was recognized in 2010 as the Outstanding Teaching Assistant in the Electrical and Computer Engineering Department.

Xiaolei Fu received the B.S. degree in electrical engineering from Zhengzhou University, Zhengzhou, China in 2003, and the M.S. degree in communication engineering from Chongqing University, Chongqing, China, in 2007. He is currently working toward the Ph.D. degree with the Department of Electrical and Computer Engineering at the New Jersey Institute of Technology (NJIT), Newark.

Since 2007, he has been working as a Research Assistant at NJIT. He has previous research experience on MIMO systems and continuous phase modulation (CPM) with the National Science Committee and General Staff of PLA, China, respectively, at Chongqing University. His current research interests include multi-spectral imaging, image reconstruction, genetic algorithms, image restoration and multi-variant optimization.

Mr. Fu was awarded the Chongqing University Freshman Scholarship in Mathematics in September 2004 and was selected as an Outstanding Graduate Student with the College of Communication Engineering, Chongqing University in November 2006.